UNIVERSIDADE FEDERAL DO CEARÁ

INSTITUTO DE CIÊNCIAS DO MAR

PROGRAMA DE PÓS-GRADUAÇÃO EM CIÊNCIAS MARINHAS TROPICAIS

ANTONIA RUTE BEZERRA DA COSTA

ELEMENTOS TERRAS-RARAS E GADOLÍNIO ANTROPOGÊNICO NA COSTA EQUATORIAL BRASILEIRA

FORTALEZA

2022

ANTONIA RUTE BEZERRA DA COSTA

ELEMENTOS TERRAS-RARAS E GADOLÍNIO ANTROPOGÊNICO NA COSTA EQUATORIAL BRASILEIRA

Dissertação apresentada ao Programa de Pós-Graduação em Ciências Marinhas Tropicais da Universidade Federal do Ceará, como requisito à obtenção do título de Mestre em Ciências Marinhas Tropicais. Área de concentração: Utilização e manejo de ecossistemas marinhos e estuarinos.

Orientador: Prof. Dr. Tristan Charles Clitandre Rousseau.
Coorientadora: Profa. Dra. Rozane Valente Marins.

FORTALEZA

2022

ANTONIA RUTE BEZERRA DA COSTA

ELEMENTOS TERRAS-RARAS E GADOLÍNIO ANTROPOGÊNICO NA COSTA
EQUATORIAL BRASILEIRA

Dissertação apresentada ao Programa de
Pós-Graduação em Ciências Marinhas
Tropicais da Universidade Federal do
Ceará, como requisito à obtenção do título
de Mestre em Ciências Marinhas Tropicais.
Área de concentração: Utilização e manejo
de ecossistemas marinhos e estuarinos.

Aprovada em: ___/___/_____.

BANCA EXAMINADORA

_____
Prof. Dr. Tristan Charles Clitandre Rousseau (Orientador)
Universidade Federal do Ceará (UFC)

_____
Profa. Dra. Rozane Valente Marins (Coorientadora)
Universidade Federal do Ceará (UFC)

_____
Dra. Mariany Sousa Cavalcante
Universidade Federal do Ceará (UFC)

_____
Dr. Emmanoel Vieira da Silva-Filho
Universidade Federal Fluminense (UFF)

A minha família.

AGRADECIMENTOS

Aos colegas do Laboratório de Biogeoquímica Costeira: Thays, Roanna, Wesley, Raisa, Mariany, Victor, César, Igor e Ana. A vocês eu sou imensamente grata por cada ajuda, cada conversa e pela simples presença no dia a dia que fazia eu não me sentir só.

À professora Rozane Marins por todo o apoio e confiança que deposita em mim.

Ao professor Tristan Rousseau pelo esforço e dedicação ao me orientar.

À professora Vanessa Hatje e ao CIEnAm-UFBA pelas análises dos Elementos Terras-Raras em ICP-MS.

"As águas vão e voltam, nunca correm só numa direção [como num rio]. Ele é como o sangue do nosso corpo, que pulsa sem parar. Por isso o mar deve ter um coração também, que nem a gente". Iamaxi Myky.

RESUMO

Os Elementos Terras-Raras (ETR) são um grupo de elementos com características físico-químicas muito próximas e utilizados como traçadores eficientes de processos geoquímicos em diversos ambientes como rios e estuários. O gadolínio (Gd), um dos ETR, pode entrar no ambiente aquático a partir de fontes antropogênicas como agentes de contraste usados em ressonância magnética e permite traçar a presença de esgotos. Os objetivos desse estudo foram: 1) caracterizar o comportamento dos ETRs na zona costeira de Fortaleza e no Delta do Parnaíba e, dessa forma, obter informações sobre a influência dessas regiões no fluxo fluvial destes elementos para o oceano e 2) avaliar se esgotos são rastreáveis nessas regiões. Foram observadas anomalias positivas de Gd na área do emissário submarino e em dois estuários de Fortaleza, indicando que a cidade é uma fonte significativa deste contaminante para o oceano. O Delta do Parnaíba, por sua vez, não apresentou anomalias positivas de Gd, o que indica que esta é uma região ainda não contaminada por esgotos.

Palavras-chave: Elementos Terras-Raras. Traçadores. Efluentes. Estuário.

ABSTRACT

Rare Earth Elements (REE) are a group of elements with very close physical-chemical characteristics and used as efficient tracers of geochemical processes in various environments such as rivers and estuaries. Gadolinium (Gd), one of the REE, can enter the aquatic environment from anthropogenic sources such as contrast agents used in magnetic resonance and allows to trace the presence of sewage. The objectives of this study were: 1) to characterize the behavior of REE in the coastal zone of Fortaleza and in the Parnaíba River Delta and, in this way, to obtain information on the influence of these regions on the fluvial flow of these elements to the ocean and 2) to assess whether sewage is traceable in these regions. Positive anomalies of Gd were observed in the area of the submarine outfall and in two estuaries of Fortaleza, indicating that the city is a significant source of this contaminant to the ocean. The Parnaíba River Delta, in turn, did not present positive Gd anomalies, which indicates that this is a region not yet contaminated by sewage.

Keywords: Rare Earth Elements. Tracers. Effluents. Estuary.

LISTA DE FIGURAS

LISTA DE TABELAS

SUMÁRIO

1 INTRODUÇÃO E ANTECEDENTES

Os Elementos Terras-Raras (ETRs, em inglês *REE*: *Rare Earth Elements*) são: lantânio (La), cério (Ce), praseodímio (Pr), neodímio (Nd), promécio (Pm), samário (Sm), európio (Eu), gadolínio (Gd), térbio (Tb), disprósio (Dy), hólmio (Ho), érbio (Er), túlio (Tm), itérbio (Yb) e lutécio (Lu). Esses 15 elementos possuem número atômico que varia do 57 (La) ao 71 (Lu), e apenas o Pm (Z = 61) não ocorre naturalmente e por isso não é quantificado em estudos ambientais de ETRs (HENDERSON, 1983). Podem ser classificados como Elementos Terras-Raras Leves (*LREE-Light Rare Earth Elements*, do La ao Nd), Elementos Terras-Raras Médios (*MREE-Middle Rare Earth Elements*, do Sm ao Tb) e Elementos Terras-Raras Pesados (*HREE-Heavy Rare Earth Elements*, do Dy ao Lu) (DEBERDT; VIERS; DUPRÉ, 2002).

Esses elementos se apresentam no estado de oxidação trivalente (3+), com exceção do Cério e do Európio que podem se apresentar também no estado de oxidação tetravalente (4+) e bivalente (2+), respectivamente. Os ETRs possuem propriedades químicas muito próximas devido ao preenchimento gradual da camada de elétrons 4f (DUBININ, 2004). Isso leva a uma diminuição do raio iônico conforme aumento do número atômico que é denominada de contração dos lantanídeos (HENDERSON, 1983). Essas características específicas dos ETRs ocasionam uma variação gradual de sua reatividade e isso permite que eles sejam utilizados como traçadores eficientes de processos geoquímicos em diversos ambientes como rios e estuários (GAILLARDET; VIERS; DUPRÉ, 2003; SHOLKOVITZ, 1995).

Em ambientes aquáticos os Elementos Terras-Raras se comportam conforme a regra de Oddo-Harkins. Nesta, elementos de número atômico par são mais abundantes que os de número atômico ímpar. Dessa forma, quando plota-se as concentrações dos ETRs *versus* o número atômico o que se observa são padrões serrilhados (Fig. 1a) (PIPER; BAU, 2013). Para facilitar a comparação visual desses elementos em diferentes amostras, inclusive de diferentes matrizes, recorre-se a normalização. Nesse procedimento utiliza-se padrões como o *Post Archean Australian Shale* (PAAS) (MCLENNAN, 1989). O PAAS apresenta um valor médio de medidas de cada ETR, sendo considerado um bom análogo a concentração relativa desses elementos na crosta. Os teores normalizados geram os padrões de distribuição dos ETRs (Fig. 1b).

Figura 1 – Exemplo de a) padrão serrilhado e b) ETRs normalizados
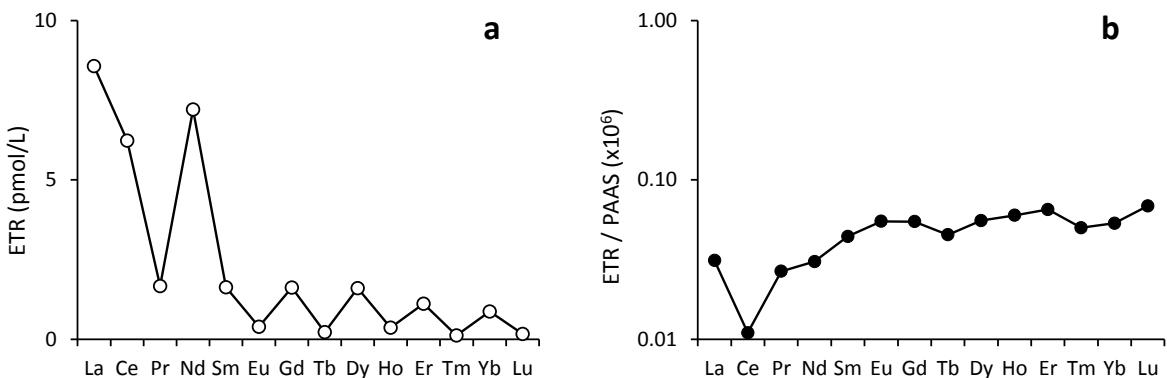
Fonte: adaptado de Deng et al. (2017).

1.1 Elementos Terras-Raras em ambientes aquáticos

A principal fonte de elementos traços para sistemas hidrológicos é a crosta continental. A introdução se dá por meio do intemperismo das rochas, da deposição atmosférica e de atividades antrópicas. Em águas continentais os ETRs são metais traços com concentrações variando de parte por trilhão (ppt) a parte por bilhão (ppb) para a fase dissolvida (GAILLARDET; VIERS; DUPRÉ, 2003). Os ETRs em água de rios podem ser associados a partículas em suspensão, associados a coloides ou verdadeiramente dissolvidos, conforme a qualidade desses materiais e a disponibilidade em abundância dos ETRs. A fração particulada é a correspondente ao material retido em filtros de 0,45 µm. A fração dissolvida é a que passa através desse filtro e pode ser separada nas frações verdadeiramente dissolvida e coloidal por meio de técnicas de ultrafiltração.

A fração verdadeiramente dissolvida é composta por ETR livre (ETR^{3+}) e por pequenos complexos de um ETR com carbonato. Os ETRs são muito reativos e tendem a formar quelatos e se associar a ânions ou a coloides minerais como oxi-hidróxidos de Fe e Mn, e orgânicos como substâncias húmicas (LEYBOURNE; JOHANNESSON, 2008; SONKE; SALTERS, 2006). Técnicas operacionais como a filtração/ultrafiltração permitem estimar essa especiação e modelos termodinâmicos têm papel fundamental para essa especiação de ETRs (TANG; JOHANNESSON, 2003).

A especiação dos ETRs varia em função de cada elemento e o comportamento geoquímico é distinto. Alguns elementos tendem a sofrer remoção do sistema aquoso em relação a outros e como consequência os ETRs apresentam uma

partição geoquímica diferenciada na fração aquosa. A fração dissolvida muitas vezes é enriquecida em *HREE* e as partículas em suspensão são enriquecidas em *LREE*. O mesmo ocorre para as frações verdadeiramente dissolvida e a coloidal. Isso é devido a retenção preferencial de *LREE* em fases sólidas, sendo os coloides os principais carreadores desses elementos (GAILLARDET; VIERS; DUPRÉ, 2003; MERSCHEL, 2015; SHOLKOVITZ, 1992, 1995).

O pH é a variável principal no controle das concentrações e fracionamento dos ETRs em ambientes aquáticos. Há uma relação inversa entre o pH e a concentração de ETRs dissolvidos em rios (Fig. 2), pois rios com baixo pH têm altas concentrações de ETRs, enquanto rios com pH alto apresentam baixas concentrações de ETRs e são enriquecidos em *HREE*. Além disso, as maiores anomalias de Ce são encontradas também em rios com altos valores de pH (GOLDSTEIN; JACOBSEN, 1988; SHOLKOVITZ, 1992).

Figura 2 – Compilação da concentração de Nd em função de valores de pH em diferentes rios do mundo
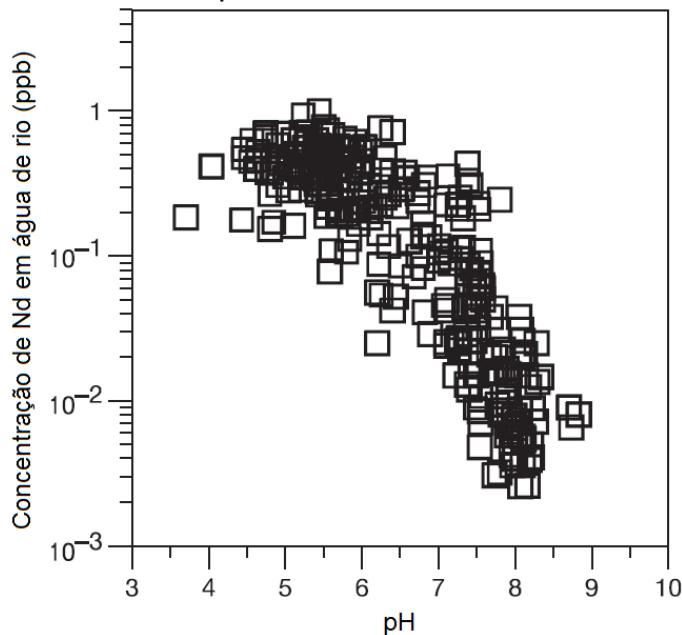
Fonte: adaptado de Deberdt; Viers; Dupré (2002).

Além do pH, salinidade, potencial redox e variações na precipitação atmosférica são variáveis que também podem influenciar na abundância e fracionamento dos ETRs dissolvidos em águas de rios (GARCÍA et al., 2007; MORA et al., 2020). O rio Orinoco, por exemplo, tem alta variabilidade de descarga e isso leva a variações consideráveis no seu pH que, por sua vez, leva a variações sazonais

nas concentrações dos ETRs. Durante períodos de baixa descarga em que o pH varia de básico a *circum*-neutro são observadas as menores concentrações de ETRs. Já as maiores concentrações são observadas durante períodos de alta descarga em que o pH é ácido naquela região (MORA et al., 2020).

Esse comportamento natural dos ETRs pode ser alterado no ambiente aquático a partir de fontes antropogênicas. Esse é o caso do Gd que tem ganhado destaque atualmente por seu comportamento anômalo em corpos hídricos e já é considerado como um contaminante emergente (KULAKSIZ; BAU, 2013). Anomalias positivas de Gd são devido ao uso de agentes de contraste à base de Gd (Gd-BCAs) em ressonância magnética (BAU; DULSKI, 1996). O Gd livre (Gd^{3+}) na corrente sanguínea é tóxico, por isso os Gd-BCAs são compostos formados pelo Gd complexado a um quelato, resistentes à ruptura por processos metabólicos e que são rapidamente eliminados por meio da excreção renal (KÜMMERER; HELMERS, 2000). Como consequência, muitos corpos hídricos que são receptores de águas residuais já apresentam um excedente de Gd denominado como Gd antropogênico (MÖLLER et al., 2000). Anomalias positivas de Gd permitem traçar a presença de esgotos e já foram observadas em rios do Brasil (DE CAMPOS; ENZWEILER, 2016). Dessa forma, o Gd antropogênico é uma ferramenta adequada para determinação da poluição por efluentes.

Os ETRs dos estuários são provenientes dos rios, portanto, em geral, a fração coloidal é enriquecida em *LREE* e a fração dissolvida enriquecida em *HREE*. Nos estuários, a presença de gradientes geoquímicos como o pH, a salinidade e força iônica alteram o equilíbrio e a estabilidade dos compostos carreados pelos rios. Os coloides sofrem coagulação e floculação, e são removidos da coluna d'água gerando fracionamento dos ETRs (SHOLKOVITZ, 1993, 1995). Esse processo de remoção ocorre em zona de baixa salinidade dos estuários. Porém, em zona de alta salinidade é possível observar um aumento nas concentrações de um *LREE* (Fig. 3). Isso é atribuído a uma liberação desses elementos de sedimentos e de partículas em suspensão (ROUSSEAU et al., 2015; SHOLKOVITZ, 1993) devido a competição das adsorções entre os ETRs e os cátions abundantes nas águas salinas. Essa liberação, no entanto, é logo neutralizada. Dessa forma, os processos que ocorrem em zona de mistura estuarina reduzem consideravelmente o fluxo fluvial desses elementos na fase dissolvida para o oceano (NOZAKI, 2001).

Figura 3 – Aumento de concentração de Nd em zona de alta
salinidade do estuário do Rio Amazonas
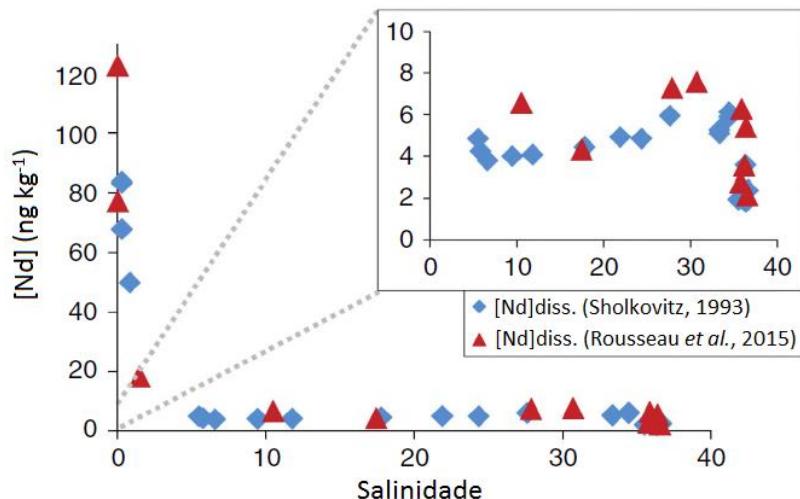
Fonte: adaptado de Rousseau et al. (2015).

Nos estuários o Ce apresenta uma alta taxa de remoção. Nesses ambientes esse elemento sofre remoção por meio da adsorção aos oxi-hidróxidos de Fe e Mn e é mais fortemente afetado pelos processos estuarinos que outros ETRs trivalentes (MERSCHEL, 2015).

Dessa forma, os estuários são responsáveis por uma remoção em larga escala de ETRs dissolvidos que adentram nos oceanos por meio do fluxo fluvial, seja por mudanças da hidroquímica, ou por processos de diluição das águas fluviais pela água do mar. Estudos de ETRs nesses ambientes de transição contribuem para o entendimento da interação continente-oceano e de como os processos que ocorrem durante essa interação afetam o aporte de elementos para o ambiente marinho.

A maior fonte de ETRs para o oceano são os rios. O tempo de residência dos ETRs no oceano é relativamente curto e para o Nd é estimado entre 200 e 1000 anos, por exemplo (TACHIKAWA; JEANDEL; ROY-BARMAN, 1999). O curto tempo de residência é ocasionado pela forte reatividade dos ETRs e pela presença de processos e mecanismos que contribuem em retirar os ETRs da coluna d'água mantendo seus teores baixos. A concentração dissolvida na água do mar de um perfil coletado no Pacífico Norte oeste é de 7.3 pmol/kg para o La e 0.3 pmol/kg para o Lu em superfície, e de 39 pmol/kg para o La e 1.5 pmol/kg para o Lu no fundo. O perfil de concentração dos ETRs é de tipo nutriente com uma leve depleção na superfície e um suave aumento com a profundidade (Fig. 4), demonstrando que estes elementos possuem uma íntima relação com o processo de produção/mineralização da matéria orgânica. Esta distribuição vertical não é observada para o Eu e o Ce (ALIBO; NOZAKI,

1999; SMRZKA et al., 2019). Devido à alta concentração de carbonato, a maior fração dos ETRs na água do mar está presente como complexos de carbonato (SHOLKOVITZ; LANDING; LEWIS, 1994).

O padrão de distribuição dos ETRs típico da água do mar é marcado pela presença de anomalias negativas de Ce (Fig. 5 elipse) e pelo enriquecimento nos *HREE* (Fig. 5 quadrado). As anomalias negativas de Ce ocorrem quando na água do mar em condições óxicas o Ce (III) é oxidado para Ce (IV) insolúvel e retirado da fração dissolvida levando ao fracionamento. Os *HREE* acabam se tornando mais concentrados devido a remoção preferencial dos *LREE* por *scavenging* que é um processo de remoção por associação às partículas em suspensão que ocorre em águas superficiais (ALIBO; NOZAKI, 1999; SHOLKOVITZ; SHEN, 1995; SMRZKA et al., 2019).

Figura 4 – Perfis de ETR na água do mar para os elementos lantânio, lutécio, európio e cério
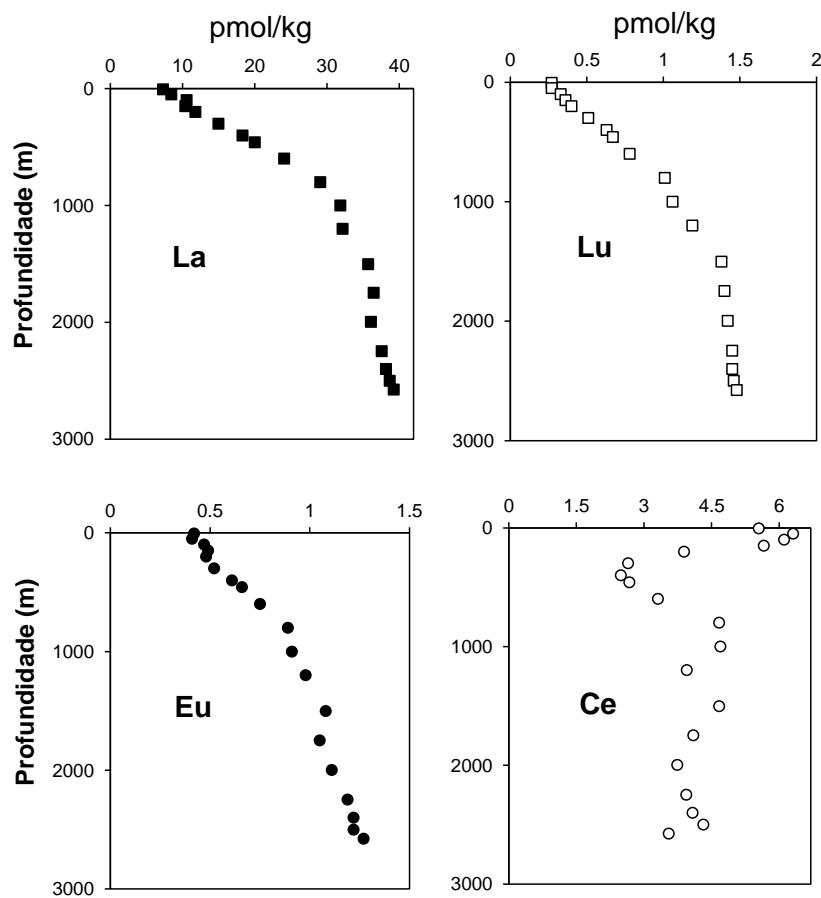
Fonte: adaptado de Alibo; Nozaki (1999).

Figura 5 – Padrões de distribuição de ETRs em água do mar
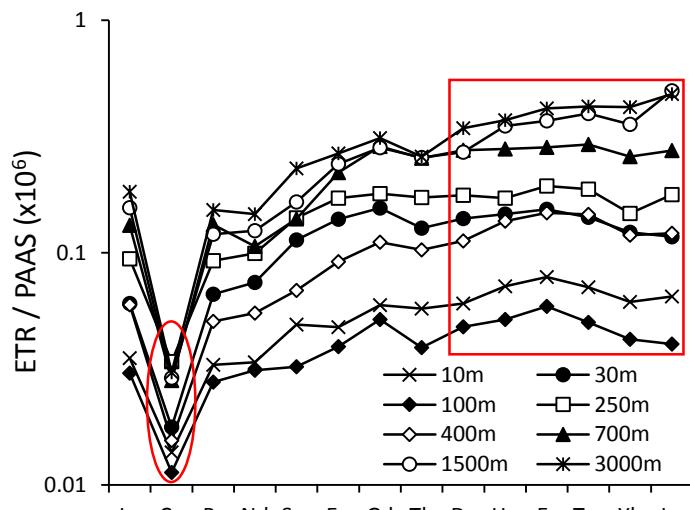
Fonte: adaptado de Deng et al. (2017).

2 HIPÓTESE

Os Elementos Terras-Raras dissolvidos aportados para o oceano pelo fluxo fluvial têm sua mobilidade influenciada pelos diferentes processos estuarinos. Os coloides são os principais carreadores desses elementos. O Gd servirá como indicador da contaminação por lançamento de esgotos nos corpos hídricos.

3 OBJETIVOS

3.1 Objetivo geral

Caracterizar a distribuição e o fracionamento geoquímico dos Elementos Terras-Raras na interface continente-oceano em Fortaleza e no sistema aquoso do Delta do Parnaíba.

3.2 Objetivos específicos

- Avaliar a influência do gradiente estuarino sobre a partição dos ETRs;
- Comparar o comportamento dos ETRs no rio Cocó, no riacho Maceió, no rio Ceará e na região de descarga do emissário submarino em Fortaleza;
- Comparar o comportamento dos ETRs no canal principal, no sistema de canais de maré e baías, em relação a variabilidade hidroquímica ao longo do Delta do Parnaíba;
- Determinar se já há presença de anomalias positivas de Gd que indiquem contaminação antrópica.

4 RESULTADOS E DISCUSSÃO

4.1 Anthropogenic gadolinium in estuaries and tropical Atlantic coastal waters from Fortaleza, Northeast Brazil

Autores: Antonia Rute B. da Costa[a], Tristan C. C. Rousseau[a], Poliana D. Maia[b], Artur M. Amorim[c], Fernando F. Sodré[c], Carlos Eduardo P. Teixeira[a]

[a] Instituto de Ciências Do Mar, Universidade Federal Do Ceará, Fortaleza, CE, CEP 60165-081, Brazil

[b] Faculdade de Planaltina, Universidade de Brasília, Área Universitária N.1, Vila Nossa Senhora de Fátima, Planaltina, 73300-000, Brazil

[c] Instituto de Química, Universidade de Brasília, Brasília, DF, CEP 70297-400, Brazil

4.1.1 Abstract

Gadolinium-based contrast agents are worldly used for medical magnetic resonance imaging and are an emerging contaminant in natural waters. We investigated the dissolved fraction of Gd in coastal waters from Fortaleza city and observe positive Gd anomalies in the wastewater outfall area as well as in two local river estuaries indicating that the city is a significant source of anthropogenic Gd (Gd_{anth}) to the ocean. Based on this synoptic study and on the conservative behavior of Gd_{anth} we trace a highly concentrated sewage-based source which accounts for 2200 pmol.kg^{-1} and to an annual discharge of 25 kg of Gd to the ocean. We also trace minor sources from the two rivers and estimate that the levels of wastewater dilution within freshwater prior to mixing with seawater accounted for 4.8% to 14% of the Cocó River discharge and 1.4% to 3.9% of the Ceará River discharge at the time of the sampling. Gd is consequently a suitable and promising tracer for water management and forensic purposes in Fortaleza. In order to guide the application of this method to other coastal waters impacted by metropolitan areas in the world, we propose a conceptual model

for Gd_{anth} behavior within salinity gradients and apply it to revisit previous studies.

Keywords: Rare earth elements; Anthropogenic Gd; Emerging contaminant; Sewage outfall; Coastal waters; Source tracer

4.1.2 Introduction

Rare earth elements (REE) form a group of elements of similar physical-chemical properties due to the gradual filling of their 4f electronic shell. Their increase in atomic number is associated with a decrease in ionic radii (Henderson 1984) leading to coherent behavior with subtle variations in reactivity and relative abundance (Sholkovitz, Landing, and Lewis 1994, Coppin et al. 2002; Luo and Byrne 2004; Köhler et al. 2005), being therefore, suitable geochemical tracers of sources and processes in rocks and aqueous media. In contrast with strictly trivalent REE, cerium and europium exist in tetravalent and bivalent respectively, in aquatic solution. Thus, they can fractionate substantially compared to their neighbors forming a naturally occurring anomaly (Elderfield 1988).

Anomalous gadolinium concentrations were first observed in samples from the Rhine River (Bau and Dulski 1996) and have since been reported in several aquatic environments located in densely populated areas around the world (Nozaki et al. 2000; Bau et al. 2006; Lawrence 2010; Hatje et al. 2016; Mortatti and Enzweiler 2019). Such anomalies can reach several orders of magnitude higher than the background Gd concentrations and are linked to anthropogenic sources related to medical activities. Gd-based contrast agents (Gd-CAs) are extensively used for magnetic resonance imaging (MRI) exams since their first approval in 1988 (Zhou and Lu 2013). As free Gd^{3+} in the bloodstream is toxic, Gd-CAs consist of chelate molecules resistant to rupture by metabolic processes and being rapidly eliminated through renal excretion (Oksendal and Hals 1993; Kümmerer and Helmers 2000; Pałasz and Czekaj 2000; Shellock 2000; Feng et al. 2010; Xia et al. 2011). Natural levels of Gd in several water bodies, used as wastewater receptors, have been exceeded (Möller et al. 2000) leading, in some regions, to contamination of soils and adjacent aquifers used as drinking water sources (Schmidt et al. 2019).

This exceeding Gd behaves conservatively and is rarely removed in wastewater treatment plants (Rabiet et al. 2014). This behavior is ascribed to the fact

that Gd ligands have a high complexation capacity with Gd and shall be non-reactive with surfaces and suspended sediments, refractory to pH variation range of different media (blood, continental water and seawater) and to bacterial activity (Schijf and Christy 2018). The conservative behavior of Gd complexes allows to trace pollution sources associated with treated and untreated wastewaters and levels of Gd may depend on population density, the numbers of MRI exams which are growing worldwide and wastewaters dilution by natural waters (Möller et al. 2000; Bau et al. 2006; Kulaksız and Bau 2007; Lerat-Hardy et al. 2019). This behavior contrasts with natural Gd and other REE which are highly reactive and tend to associate with organic and mineral colloidal ligands removed from the water column in estuaries (Sholkovitz 1993; Rousseau et al. 2015). To date, the toxicity of this emerging contaminant and its long-term lability are still poorly known (Henriques et al. 2019; Fujita et al. 2020) and its levels have shown a significant increase over short periods of time in some locations (Tepe et al. 2014; Hatje et al. 2016).

In a recent study, Pedreira et al. (2018) observed the presence of Gd anomalies in coastal waters near the outfalls of two WWTP from Salvador city, northeast Brazil. The authors measured the anthropogenic Gd concentration within these WWTPs and used national wastewaters discharges data to perform a mass balance of its load exported annually by Brazilian coastal cities outfalls. The present work was developed in Fortaleza city, the capital of Ceará state located in the northeast region of the country (Figure 6). Fortaleza is the fifth Brazilian city in population size and has 35 magnetic resonance facilities, i.e., 1.3 equipment per 100000 inhabitants (Datasus 2019), which is close to the 1.6 average ratio observed for the Organization for Economic Co-operation and Development countries (OECD 2020). Serving as a regional medical pole, Fortaleza receives patients from distant areas and faces a high demand on these equipments, since the entire Ceará state, with an area of nearly 149000 km^2, has 55 magnetic resonance facilities, 0.3 equipment per 100000 inhabitants.

Fortaleza discharges its wastewaters primarily by a submarine outfall located 3.2 km from the shoreline and secondly in two small rivers which cross the city which are under pressure of distinct human activities such as navigation, fishing and recreational activities. Here we investigated the concentrations of dissolved REE in Fortaleza estuaries and coastal waters in order to check whether Fortaleza medical activities lead to detectable anthropogenic Gd, to investigate potential wastewater-

derived sources of contamination and to refine earlier mass balance calculations.

4.1.3 Materials and methods

4.1.3.1 Study area

Fortaleza climate is influenced by the Intertropical Convergence Zone (ITCZ) experiencing contrasted seasonal trade winds and rainfall regimes (Ferreira and da Silva Mello 2005). According to the national institute of meteorology (INMET 2019), 90% of the average total precipitation (1432 mm/year) occurs between January and June when the winds are relatively weak. Contrastingly, the period from July to December is dry and the winds are stronger. The prevailing winds are oriented WNW and generate average coastal currents parallel to the coast (Pereira et al. 2015). This circulation pattern has a relatively constant direction throughout the year as shown in Figure 6a.

The city has approximately 2.7 million inhabitants (IBGE 2019) of which 61% have their wastewaters collected and treated (ANA 2017). Three water bodies cross the urban zone and receive treated and raw wastewaters discharges (Nilin et al. 2013): Cocó River, Ceará River and Maceió Stream (Figure 6b). A high-capacity preliminary WWTP collects and treats 49% of the wastewaters produced by Fortaleza and discharges the effluents through a submarine outfall built in the seventies. It is 3.2 km long, has a 1.5 m diameter and operates a 2.2 $m^3.s^{-1}$ discharge at a 12m depth (CAGECE 2014). The coastal circulation maintains the wastewater plume distant from the shoreline and advects it parallel to the coast. In contrast, the waters from the Cocó and Ceará rivers, the Maceió Stream and the 32 storm sewers distributed alongside the city seafront are advected westwards but relatively close to the coast (Pereira et al. 2015).

Figure 6 – Study area and sampling stations: a) Ceará state localization and Fortaleza coastal circulation scheme (current direction adapted from Pereira et al. 2015) b) Four areas were covered in this study: Cocó River (samples 1 to 6), Maceió Stream (samples 7 to 10), Fortaleza outfall (sample 11 to 14) and Ceará River (Sample 15 to 21). The dashed line represents the localization and extension of Fortaleza submarine outfall and the star the localization of the mmajor WWTP
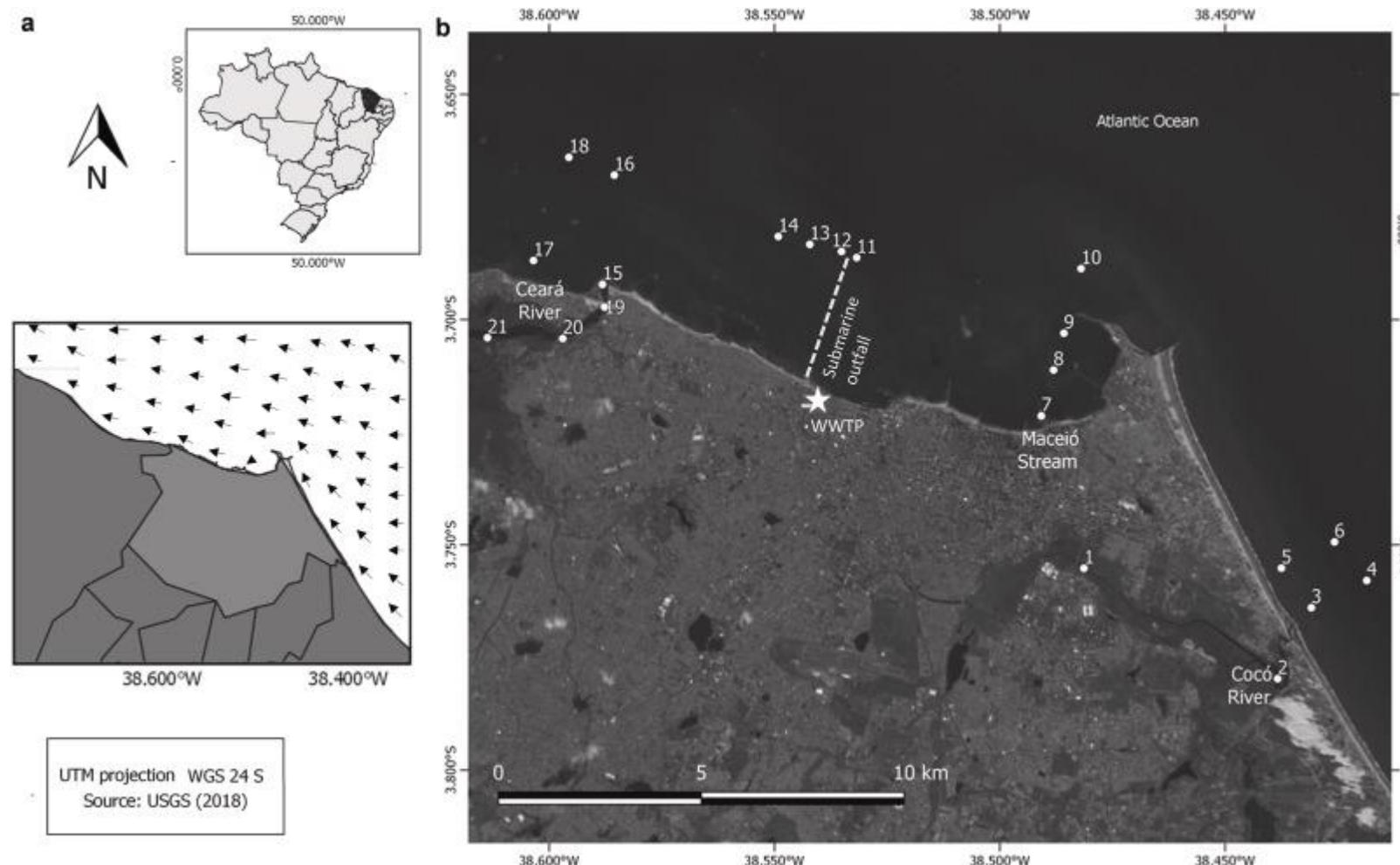
4.1.3.2 Sampling

A total of 19 nearshore surface water samples were collected in April and May 2018 in areas under the influence of the Cocó and Ceará rivers, the Maceió Stream and the submarine outfall of Fortaleza (Figure 6). Sampling points were chosen considering prevailing winds, water circulation and the subsequent urban water dispersion. Two bottom samples were also obtained at 12m in the outfall discharge area. Samples within the Cocó and Ceará rivers were also collected. Van Dorn bottles were used for sample collection and HCl cleaned 1L high-density polyethylene (HDPE) bottles were used for sample storage. Samples were filtered with pre-cleaned 0.45 µm cellulose ester mixed membranes (Millipore, Merck) and acidified with doubly distilled HCl (Quartz Sub-boiling distiller) to pH 2. Temperature and salinity data were acquired with an in situ multiparametric probe (EXO2, Ysi).

4.1.3.3 Analytical procedures

C18 solid-phase extraction cartridges (Sep-Pak, Waters), loaded with 2-ethylhexyl phosphate (HDMEP-H2DMEP), were used for REE preconcentration and salts removal (Shabani et al. 1992; Merschel et al. 2015; Amorim et al. 2019). Briefly samples were acidified, spiked and kept for a two months and a half period at ambient air conditioning lab temperature. Subsequently samples were loaded through the C18 cartridges with a peristaltic pump at a flow rate of 9 mL min^{-1}. Prior to the REE elution, the cartridges were washed with 10 mL of HCl 0.01 mol.L^{-1} at a flow rate of 3 mL min^{-1} to remove some major elements including the interfering Ba. Then, the analytes were eluted with 40 mL of HCl 5.6 mol.L^{-1}, at a flow rate of 3 mL min^{-1}. The eluate was evaporated in pre-cleaned 60-mL PFA vials on a heating plate until dryness and the remaining material was dissolved back in 5 mL of a 0.32 mol.L^{-1} HNO$_3$. All acids used in this extraction procedure were double-distilled.

Quantification of REE was carried out in an Agilent 7500ce inductively coupled plasma mass spectrometer (ICP-MS) according to analytical procedure for data treatment and interference monitoring/corrections proposed elsewhere (Rousseau et al. 2013; Amorim et al. 2019). REE concentrations were determined by isotopic dilution using a mix of ^{146}Nd, ^{151}Eu, and ^{172}Yb spikes added to the samples before the preconcentration step. In each individual sample the recoveries were

monitored and corrected for Nd, Eu and Yb and interpolated for non-spiked REE. On average, Nd, Eu and Yb showed recoveries of 83%, 88%, and 86%, respectively. Blanks were inferior to 6% for heavy REE (HREE) and 3% for middle REE (MREE). For light REE (LREE) such as La, Ce, and Pr, blank correction reached about 10% of the signal in some samples. The methods for sample preparation and analyses used in this study were successfully applied the analyses of the SLRS-6 river water reference material (Amorim et al. 2019; Yeghicheyan et al. 2019). Considering the higher salinity of the samples investigated in the present study compared to SLRS-6, the matrix separation efficiency was checked by analyzing Na and Ca by Inductively Coupled Plasma Optical Emission Spectrometry (Thermo iCAP 6000 Series) and showed that preconcentrated samples had Na and Ca concentrations 10^6 and 2.10^2 times lower than seawater respectively. As discussed by de Campos and Enzweiler (2016) chelated Gd used as contrast agents can have low retention in C18 cartridges. Since our samples were kept acidified for a long period before preconcentration we assume good recoveries for this element. More analytical developments are however necessary in the field and specially to insure fully quantitative Gd recoveries for sea water. For example, a recent study on tap waters and soda samples by Schmidt et al. (2019) have shown good recoveries when adding a H_2O_2 digestion step prior to the acidification step.

4.1.4 Results

Table 1 shows the salinity, temperature and REE concentrations for the samples collected within the scope of this study. Temperature varied between 28.9 and 30.0 °C, salinity ranged from 0.3 for sample 1 (Cocó River estuary) to 36.0 for sample 15. Most of the coastal samples displayed salinities between 35.6 and 36 except for station 5 (32.8) which is influenced by the Cocó River plume. The saltiest samples presented values between 35.9 and 36.0 and can be considered as the marine endmember. Slightly fresher waters were observed for samples 11 and 12 (35.7 and 35.7, respectively) which are surface water samples located in the sewage outfall region characterized by a wastewater plume. Lower salinities were observed in Ceará River estuary (samples 19, 20 and 21; salinity 6.1, 7.8, and 19.2, respectively).

Table 1 – Sampling localization, hydrographic data and rare earth elements concentrations (pmol.kg^{-1})

Area	Sample	Date	Latitude	Longitude	Temp.	Salinity	La	Ce	Pr	Nd	Sm	Eu	Gd	Tb	Dy	Ho	Er	Tm	Yb	Lu	∑REE
Cocó River	1	04/05/18	-3.75516	-38.48132	ND	0.31	118.4	176.8	35.5	171.7	42.2	10.9	154.0	5.90	37.8	10.7	45.7	8.86	76.3	15.6	910.3
	2	04/05/18	-3.77969	-38.43835	ND	35.34	25.87	31.23	5.43	23.05	4.70	1.29	7.79	1.14	8.06	2.02	6.85	1.06	7.17	1.26	126.9
	3	09/04/18	-3.75789	-38.41856	29.5	35.65	23.25	44.75	4.97	19.41	3.93	0.96	5.34	0.85	5.76	1.40	4.51	0.70	4.28	0.77	120.9
	4	09/04/18	-3.76393	-38.43086	29.4	35.74	21.71	42.07	4.41	17.64	3.66	1.00	5.10	0.80	5.38	1.21	4.26	0.65	4.00	0.64	112.5
	5	09/04/18	-3.75514	-38.43750	30.0	32.76	27.96	53.87	5.69	24.80	5.32	1.37	9.32	1.01	7.11	1.75	6.17	0.98	7.20	1.29	153.8
	6	09/04/18	-3.74932	-38.42572	29.3	35.84	18.12	36.19	3.46	12.73	2.86	0.75	3.61	0.57	4.02	0.95	3.10	0.46	2.99	0.51	90.3
Maceió Stream	7	13/04/18	-3.72134	-38.49077	29.4	35.94	26.03	41.11	4.83	19.52	3.91	1.05	6.12	0.89	6.30	1.53	5.25	0.81	5.41	0.89	123.6
	8	13/04/18	-3.71116	-38.48806	29.1	35.94	24.69	39.46	4.85	21.13	4.11	1.05	6.58	0.94	6.64	1.60	5.29	0.79	5.10	0.83	123.0
	9	13/04/18	-3.70299	-38.48577	28.9	36.01	24.99	40.25	4.82	19.53	4.02	1.06	6.14	0.92	6.48	1.55	5.19	0.78	5.30	0.83	121.9
	10	13/04/18	-3.68866	-38.48196	28.9	35.95	19.31	34.70	3.67	14.49	3.15	0.77	4.11	0.65	4.48	1.06	3.44	0.55	3.39	0.56	94.31
Fortaleza Outfall	11S	12/04/18	-3.68622	-38.53176	29.0	35.71	18.80	43.61	4.83	18.54	3.74	0.95	17.40	0.78	5.08	1.21	3.82	0.55	3.56	0.61	123.5
	11D	12/04/18	-3.68622	-38.53176	28.9	35.91	37.28	59.97	4.09	16.01	3.33	0.97	4.77	0.77	4.93	1.23	3.99	0.60	3.77	0.64	142.3
	12S	11/04/18	-3.68485	-38.53512	28.9	35.69	16.95	50.21	5.75	24.89	4.86	1.21	24.08	0.89	6.02	1.44	4.41	0.68	4.29	0.76	146.4
	12D	11/04/18	-3.68485	-38.53512	28.9	35.95	18.44	39.37	4.22	16.33	3.46	0.84	5.20	0.70	4.97	1.13	3.81	0.56	3.58	0.58	103.2
	13	11/04/18	-3.68327	-38.54216	29.1	35.75	16.08	42.28	4.82	20.95	4.18	1.10	16.88	0.83	5.40	1.28	4.22	0.65	4.13	0.67	123.5
	14	11/04/18	-3.68152	-38.54915	29.1	35.79	22.98	53.83	5.29	20.90	4.13	1.12	14.95	0.82	5.20	1.26	3.98	0.58	3.84	0.65	139.5
Ceará River	15	10/04/18	-3.69215	-38.58816	29.6	36.02	31.07	55.83	5.72	23.07	4.90	1.37	6.75	1.07	7.07	1.76	5.68	0.87	5.58	0.93	151.7
	16	10/04/18	-3.66790	-38.58555	29.3	35.98	21.96	42.45	3.83	14.39	3.06	0.81	4.04	0.62	4.14	0.99	3.19	0.49	3.00	0.50	103.5
	17	10/04/18	-3.68684	-38.60349	29.6	35.71	36.35	65.46	6.74	27.32	5.52	1.35	9.09	1.10	7.55	1.82	5.95	0.88	5.98	1.03	176.1
	18	10/04/18	-3.66395	-38.59563	29.34	35.60	26.47	49.44	5.76	23.27	4.73	1.30	8.61	1.04	6.09	1.50	4.67	0.81	4.65	0.90	139.3
	19	08/05/18	-3.69718	-38.58772	ND	19.22	39.65	58.91	8.44	35.93	7.30	1.93	11.02	1.38	9.27	2.23	7.96	1.30	9.11	1.71	196.1
	20	08/05/18	-3.70418	-38.59700	ND	7.79	272.3	663.9	67.1	282.8	53.4	12.97	62.10	7.31	41.85	9.21	30.68	5.07	38.29	7.50	1555
	21	08/05/18	-3.70399	-38.61369	ND	6.06	287.7	697.6	71.4	298.8	58.0	13.51	68.59	7.89	44.61	9.88	32.59	5.45	40.89	8.04	1645

4.1.4.1 Rare earth elements

The sum of all REE concentration ($\sum$REE) varied from 90.3 pmol.kg^{-1} (coastal sample 6) to 1644 pmol.kg^{-1} (sample 21). The highest $\sum$REE concentration were observed for Cocó and Ceará River estuaries which also presented low salinity (samples 1, 20 and 21). Post-Archean Australian Shale (PAAS) normalized REE diagrams (McLennan 1989) are reported in Figure 7. Samples 1, 20 and 21, which presented the highest $\sum$REE levels, also showed REE distribution patterns with a substantial offset compared to the other samples (Figure 7a, 7d). All REE distribution patterns displayed a gradual fractionation, from depleted LREE to enriched HREE. Atlantic Ocean waters usually display such typical fractionated behavior. Therefore, La$_{sn}$/Yb$_{sn}$ ratios presented in Table 2 were systematically inferior to 1, varying from 0.09 for sample 1; with the lowest salinity sampled for Cocó River; to 0.59 for sample 11D located nearby the submarine outfall. Looking into detail, for most samples, however, REE patterns were rather flat from La to Nd and then increased from Nd to HREE. Sample 11D presented an enrichment in La (Figure 7b) with a La$_{sn}$/Nd$_{sn}$ ratio of 2 (Table 2). Cerium anomaly (Ce/Ce*) was calculated following equation 1:

$$\frac{Ce}{Ce^*} = \frac{Ce_{sn}}{(La_{sn} \times Pr_{sn})^{0.5}}$$

Eq. 1

where Ce* is the estimated non anomalous cerium concentration, Ce$_{sn}$, La$_{sn}$ and Pr$_{sn}$ are the PAAS normalized REE concentrations. Ce/Ce* were on average 0.97 ± 0.16 and varied from 0.61 for Cocó River (sample 2) to 1.18 for sample 12S in the outfall area (Table 2). Samples 10 and 6 presented the lowest REE concentrations, with distribution patterns close to a sample collected by Rousseau et al. (2015) over the same continental margin further west at 90 m depth close to the Amazonian shelf break (Latitude: 2,26 ºS e Longitude: -47,50 ºW) (Figure S1). Despite this similarity in REE patterns, Ce displays a different behavior and while samples 6 and 10 indicate the absence of Ce anomaly (1.06 and 0.95, respectively) the sample reported for comparison displayed a large negative anomaly (0.5).

Figure 7 – PAAS normalized rare earth elements patterns in the areas
investigated in this study: a) Cocó river, b) Maceió stream,
c) Fortaleza submarine outfall, d) Ceará River
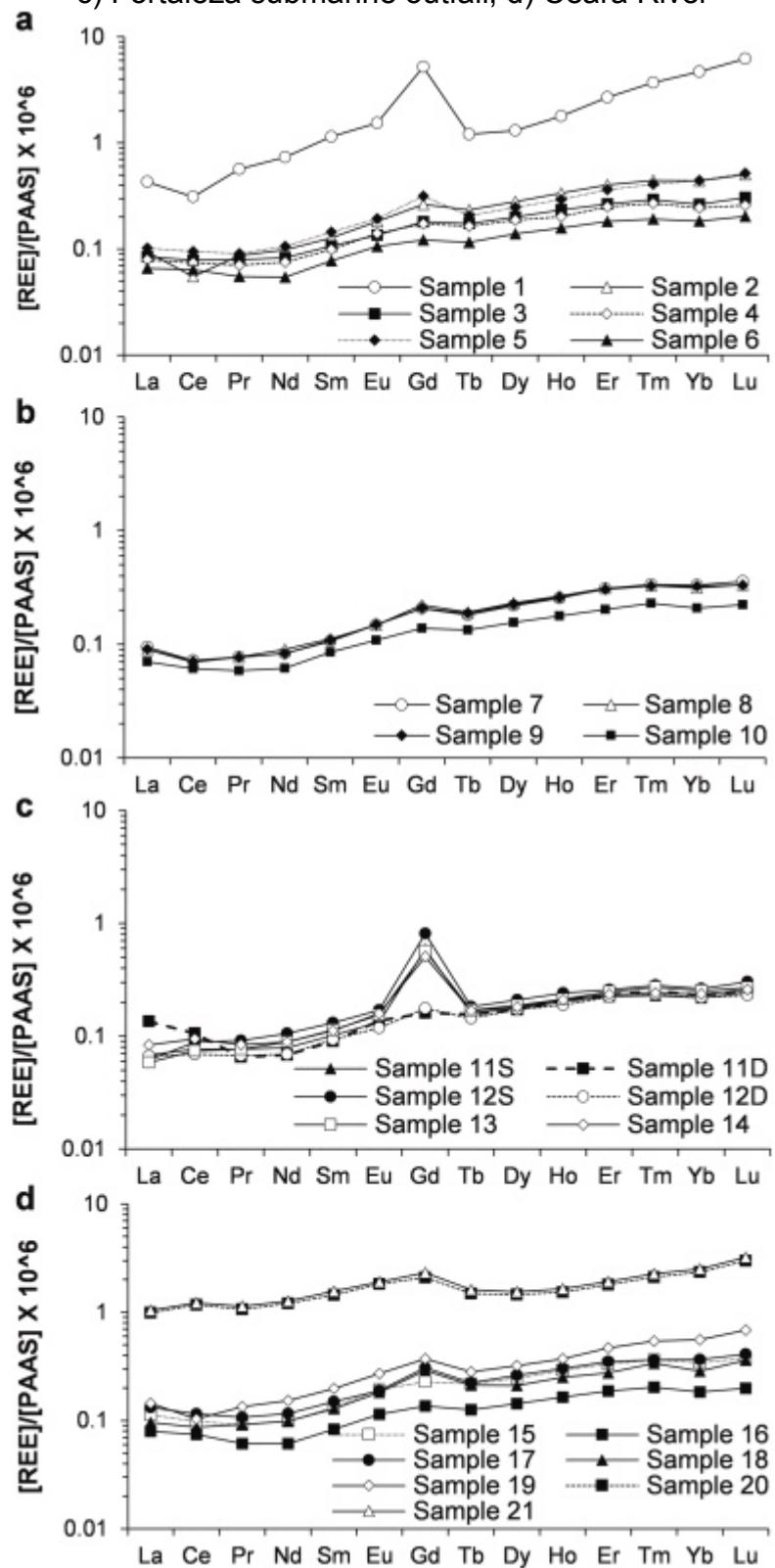
Table 2 – Post Archean Australian Shale (PAAS) normalized REE ratios, Ce and Gd anomalies, and anthropogenic Gd concentration (Gd$_{anth}$) expressed in pmol.kg^{-1}

Area	Sample	$\dfrac{La_{sn}}{Yb_{sn}}$	$\dfrac{La_{sn}}{Nd_{sn}}$	$\dfrac{Ce_{sn}}{Ce_{sn}^*}$	$\dfrac{Gd_{sn}}{Gd_{sn}^*}$	Gd$_{anth}$
Cocó River	1	0.09	0.59	0.63	5.4	125.37
	2	0.21	0.96	0.61	1.3	1.77
	3	0.32	1.02	0.96	1.2	0.76
	4	0.32	1.05	0.99	1.2	0.84
	5	0.23	0.96	0.99	1.7	3.88
	6	0.36	1.22	1.06	1.2	0.50
Maceió Stream	7	0.29	1.14	0.85	1.3	1.36
	8	0.29	1.00	0.83	1.3	1.46
	9	0.28	1.09	0.85	1.2	1.20
	10	0.34	1.14	0.95	1.2	0.57
Fortaleza Outfall	11S	0.31	0.87	1.06	4.1	13.18
	11D	0.59	1.99	1.12	1.3	1.01
	12S	0.23	0.58	1.18	4.7	18.94
	12D	0.30	0.97	1.03	1.3	1.27
	13	0.23	0.66	1.11	3.7	12.28
	14	0.35	0.94	1.13	3.4	10.53
Ceará River	15	0.33	1.15	0.97	1.2	1.11
	16	0.43	1.3	1.07	1.2	0.72
	17	0.36	1.14	0.97	1.5	3.14
	18	0.34	0.97	0.93	1.7	3.47
	19	0.26	0.94	0.74	1.5	3.73
	20	0.42	0.82	1.14	1.6	22.04
	21	0.42	0.82	1.13	1.6	25.58

4.1.4.2 Gd anomaly

REE patterns presented an anomalous Gd behavior in many samples as it is offset from the smooth increasing trend in REE patterns (Figure 7a-d). Several methods allow the numerical evaluation of the Gd anomaly by estimating the background shale normalized concentration (Gd$_{sn}^*$) of this element (Hatje et al. 2016). Gd$_{sn}^*$ can be estimated by fitting, for each sample, a third-order polynomial of PAAS normalized REE values against their discrete ranking (from one to fifteen) and solving the equation for the Gd position (Figure S2). This multiple regression method disregards potentially anomalous elements (Gd, Ce, and Eu). It is advantageous for not considering Gd as LREE nor HREE and thus more appropriated when comparing the range of REE patterns found between freshwater and seawater (Möller et al. 2002; Hatje et al. 2016). Gd anomaly (Gd$_{sn}$/Gd$_{sn}^*$) was calculated following equation 2:

$$\frac{Gd_{sn}}{Gd_{sn}^*} = \frac{Gd_{sn}}{(\beta_3 x^3 + \beta_2 x^2 + \beta_1 x + \beta_0)} \qquad \text{Eq. 2}$$

where Gd_{sn} is the PAAS normalized gadolinium concentration and Gd_{sn}^* is calculated by solving each fitted third-order polynomial of β_0, β_1, β_2 and β_3 parameters for x=8 (gadolinium position). For low Gd_{sn}/Gd_{sn}^* values the anomaly can sometimes be hardly distinguishable from natural Gd levels as this REE is located between LREE and HREE which may have contrasted reactivity and fractionation patterns and because of possible analytical uncertainties in REE determination. As a result, it is important to consider low positive Gd anomalies with caution and a threshold for Gd_{sn}/Gd_{sn}^* between 1.3 and 1.5 is usually chosen arbitrarily to attribute the anomaly to anthropogenic activities (Pedreira et al. 2018; Andrade et al. 2020). In our study considering $Gd_{sn}/Gd_{sn}^* \geq 1.3$, 16 samples presented a Gd anomaly and considering $Gd_{sn}/Gd_{sn}^* \geq 1.4$, 11 samples presented this anomaly (Table 2). The sample from the Cocó River presenting the lowest salinity (sample 1) also displayed the highest Gd/Gd^* anomaly. In the coastal area influenced by the Cocó River estuary, only sample 5 displayed an anomalous behavior. In the Ceará River, estuarine samples 19, 20 and 21 and coastal samples 17 and 18 displayed a positive anomaly. In the Maceió Stream coastal area, samples 7 and 8 showed a slight positive anomaly. All the surface samples in the outfall area presented a significant positive anomaly ranging from 3.4 to 4.1, it is comparable with the value of 3.4 found by Pedreira et al. (2018) for the outfall plume of Salvador city.

4.1.4.3 Robustness of the polynomial method for Gd* estimates

Since La can eventually present an anomalous behavior compared to other LREE (Kulaksız and Bau 2011; Garcia-Solsona et al. 2014; Klaver et al. 2014; Amorim et al. 2019) we made a sensitivity test in order to evaluate any possible influence of La variations on Gd^* estimations (Figure S3a). For sample 3, a -50% and +50% variation of La value leads to a 3.5% variation of Gd^* in the opposite direction (Figure S3b). Consequently, this third order polynomial method can be applied thoroughly for Gd* estimations except in the presence of very high La anomalies (i. e., more than 10-fold the non anomalous concentration). In our study, La behavior was quite constant for most of the samples with narrow variations of La_{sn}/Pr_{sn} (1.10 ±0.27). The only sample

showing a contrasted La behavior was sample 11D (Figure 7c), which presented a La_{sn}/Pr_{sn} ratio of 2 and a slightly anomalous Gd/Gd* ratio of 1.3. If we fit a polynomial for this sample using a hypothetical La_{sn} value using the average La_{sn}/Pr_{sn} value of 1.05 we find a different Gd/Gd* of 1.6. Beside this exception where the Gd anomaly could be slightly underestimated, the polynomial method is suitable and allows us to compare our data with other studies (Hatje et al. 2016; Pedreira et al. 2018; Andrade et al. 2020).

4.1.5 Discussion

4.1.5.1 Fortaleza as a traceable source of anthropogenic Gd

The Gd/Gd* values we observe ranged from 1.2 to 5.4 and are comparable with previously reported values in coastal waters near Salvador (Gd/Gd* ranging from 1 to 3.4; Pedreira et al. 2018) but substantially lower than values observed in continental waters near other Brazilian metrocities like Campinas city in fluvial environment (Gd/Gd* ranging from 0.8 to 86.7; De Campos and Enzweiler et al. 2016) and Brasilia´s lake (Gd/Gd* ranging from 1.1 to 68.4; Merschell et al 2015, Amorim et al 2019). Considering that the highest ratios were observed in Cocó and Ceará rivers and in the WWTP outfall region, Fortaleza unequivocally provides a traceable source of anthropogenic Gd to the ocean. Several magnetic resonance equipments are implanted in Fortaleza and this medical care activity has been the most suitable candidate to explain Gd anomalies in the waterbodies draining densely populated areas. Thus, it is likely that Gd anomalies are linked to the use of Gd-CAs.

We also observe significant Gd anomalies in samples collected westwards of the Cocó River (sample 5), the Ceará River (sample 17) and the outfall region (samples 12, 13 and 14), suggesting a Gd mobility and dispersion patterns in agreement with the ones modelled by Pereira et al. (2015). It is important to point out that as Gd/Gd* ratios relate to the background Gd concentrations they are not fully adequate for comparisons between continental waters and seawaters which display large variations in REE levels. Additionally, these elements are reactive and can be removed from the dissolved phase by scavenging and colloids flocculation or added to the system through release from sediments and suspended particles (Sholkovitz 1993; Rousseau et al. 2015; Johannesson et al. 2017).

4.1.5.2 Anthropogenic Gadolinium quantification

To overcome the effect of potentially high natural REE variation on Gd/Gd*ratios, for example between riverwater and seawater, we estimate the absolute anthropogenic gadolinium concentration (Gd_{anth}) using equation 3:

$$Gd_{anth} = Gd - (Gd_{PAAS} \times Gd_{sn}^{*})$$ Eq. 3

where Gd is the measured concentration, Gd_{PAAS} is the PAAS normalized Gd concentration, as proposed by McLennan (1989), and Gd_{sn}^{*} stands for the PAAS normalized natural Gd estimated by the polynomial fit. As shown in Figure 8 Gd_{anth} decreases as salinity increases in the outfall region (samples 10, 11S, 11D, 12S, 12D, 13, and 14) reflecting the dilution of a concentrated freshwater endmember by seawater. In the Cocó River area (samples 1, 2, and 5) and in the Ceará River area (samples 19, 20, and 21) the same dilution pattern is observed (figure S4). A remarkably linear and conservative estuarine Gd_{anth} behavior was previously reported for the entire salinity gradient in the Weser estuary (Kulaksız and Bau 2007). This is in agreement with our results in the outfall region where there was a significant negative correlation between salinity and Gd_{anth} (r(5)=0.97, p<.001). Assuming a conservative Gd_{anth} behavior over the whole salinity gradient one can infer that the wastewater endmember concentration ($Gd_{anth,wwtp}$) is the interception of the linear regression with the Y axis at 0 salinity (i. e., the $\hat{b}$ parameter). The standard deviation (s_b) of the intercept $\hat{b}$ is the square root of its variance (Equation 4):

$$s_b^2 = \frac{SS_E}{n-2} \left(\frac{1}{n} + \frac{\bar{x}^2}{SS_{xx}} \right)$$ Eq. 4

where SS_E is sum of squared estimate of errors, SS_{xx} is sum of squares of x observations. According to Eq. 4, s_b allows us to give a 95% confidence interval for $\hat{b}$ following the t-distribution with n-2 degrees of freedom. As a result, we calculate a source concentration for the Gd_{anth} signal measured in the outfall area of 2240 ± 470 pmol.kg^{-1}. This result is in agreement with the value obtained by Pedreira et al. (2018) in Salvador city, where the authors reported Gd_{anth} values measured directly in the WWTPs and varying between 900 and 2605 pmol.kg^{-1}. These values were used as

reference to estimate Gd_{anth} exported from the Brazilian coastal cities. Considering the average discharge of the submarine outfall of Fortaleza, approximately 24.6 ± 5.2 kg of anthropogenic Gd are launched to the ocean every year. It corresponds to nearly 22400 MRI exams if an average of 1.1 g of Gd is administered during each analysis in Brazil (Telgmann et al. 2013; Merschel et al. 2015; Pedreira et al. 2018). Our estimate is based on a synoptic observation and shall be considered more as an order of magnitude, indeed substantial variations in Gd concentrations can occur in WWTP within a few days according to the daily number of MRI exams (Pedreira et al. 2018).

Figure 8 – Anthropogenic gadolinium (Gd_{anth}) as function of salinity in
Fortaleza submarine outfall area
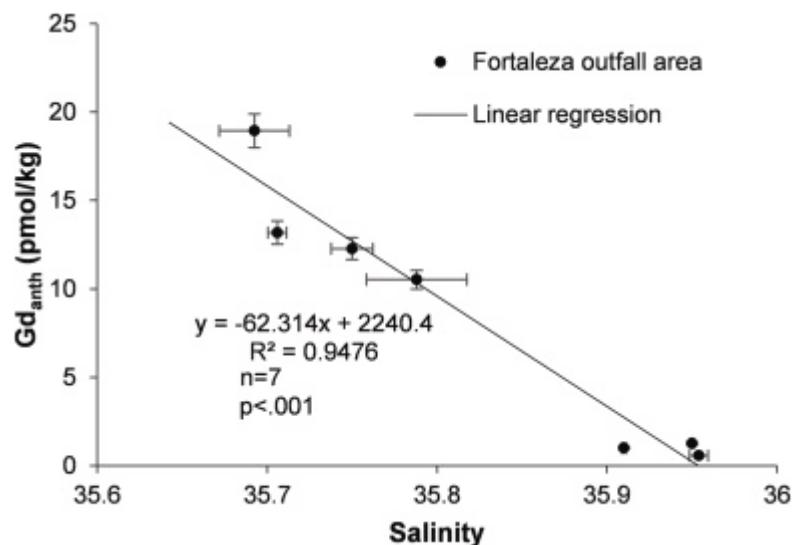
For the estuaries of Cocó and Ceará rivers, the Gd_{anth} values extrapolated to the freshwater endmember ($Gd_{anth,S=0}$) were of 126 ± 5 pmol.kg^{-1} and 35.2 ± 1.2 pmol.kg^{-1},respectively. Despite higher Gd/Gd* ratios and Gd_{anth} values within the estuary, these Gd_{anth}(0) levels are inferior to the one calculated for the submarine outfall and support the hypothesis that wastewater discharges are firstly diluted by the river waters prior to seawater/river mixing. According to the Brazilian National Water Agency (ANA 2017) Cocó and Ceará rivers receive, respectively, a total of 352 L s^{-1} and 104 L s^{-1} of treated and non-treated wastewaters. These effluents are distributed in several punctual canalizations along the watercourses. To our knowledge, yearly hydrological data are not available for both rivers and the only data accessible from the water agency is their minimum reference discharge (76.5 L s^{-1} for Cocó River and

116.6 L s^{-1} for Ceará River). As a result, during the dry season, it is estimated that wastewaters shall account for 75% and 40% of Cocó and Ceará rivers discharge. As sampling was carried out during the rainy season (April and May) both rivers shall display a substantially higher discharge than during the dry season. In this case, a simple mass balance can be applied here to estimate the river water and wastewater (%WW) proportions during the sampling period using equation 5:

$$\%WW = \frac{Gd_{anth,S=0}}{Gd_{anth,WWTP}}$$
Eq. 5

where $Gd_{anth,S=0}$ is the anthropogenic Gd estimated for the freshwater endmember and $Gd_{anth,WWTP}$ is the anthropogenic Gd concentration within the wastewater treatment plant.

Based on equation 5 and considering the minimum and maximum values for $Gd_{anth,WWTP}$ as observed by Pedreira et al. (2018), i. e., 900 to 2600 pmol.kg^{-1}, we suggest that wastewaters accounts for 4.8% to 14% of the discharge of Cocó River and for 1.4% to 3.9% of the Ceará River during the study period. Therefore, Gd$_{anth}$ is a suitable tracer to monitor the dilution of wastewaters within rivers as it is minimally influenced by wastewater treatment processes compared to other usual parameters such as biologic oxygen demand and nutrients. In addition, Gd$_{anth}$ might closely follow the fate of other conservative emerging contaminants. The submarine outfall delivers high Gd$_{anth}$ concentrations rapidly diluted by seawater. Contrastingly, for river systems, even if conservative contaminants are previously diluted within freshwater prior mixing with seawater, they might be more harmful to the biota in estuaries given their longer residence time and higher absolute concentrations.

4.1.5.3 Potential applications using Gd$_{anth}$ as a conservative tracer

In this section we develop a simple conceptual vision of Gd$_{anth}$ in salinity gradients and revisit earlier studies based on this approach. Considering the conservative behavior of Gd$_{anth}$ during freshwater/seawater mixing, three scenarios can possibly occur. In the first scenario (Figure 9a), a concentrated Gd$_{anth,\,S=0}$ source is diluted by seawater. This high Gd$_{anth}$ content is characteristic of wastewater outfalls and can be applied to evaluate endmember concentrations and fluxes or to attribute

confidently eventual slight salinity fluctuations due to the presence of diluted sewage plumes. Samples collected in the present study in the Fortaleza outfall area and in Salvador city outfall area by Pedreira et al. (2018) can be associated with this scenario.

Figure 9 – Conceptual cases illustrating the conservative behavior of anthropogenic Gd during freshwater/seawater mixing: a) highly concentrated Gd_{anth} source scenario; b) diluted Gd_{anth} source scenario and; c) two distinct sources scenarios
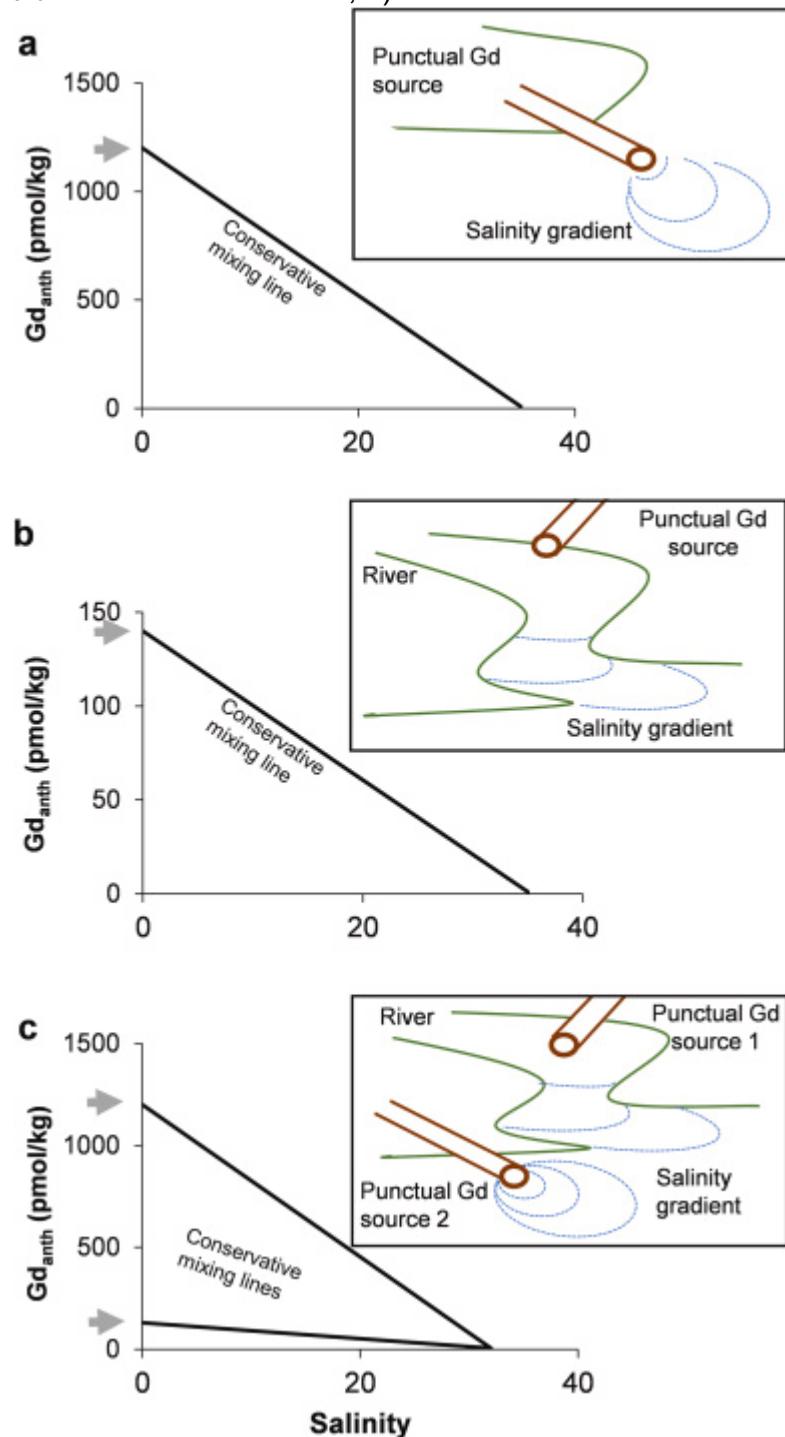
In scenario two (Figure 9b), a freshwater source with lower and homogeneous Gd_{anth} levels mixes with seawater. In this scenario, any concentrated source is mixed and diluted by freshwaters (i.e. 0 salinity) prior to mixing with seawater. This scenario is observable for river samples collected in Cocó and Ceará rivers in the present study and allows to calculate water balances. This type of estuarine mixing was also observed for the Weser estuary where seasonal variations of wastewater dilution in the freshwater endmember are observable between March 2005 (Gd_{anth} =86 ±4 pmol.kg^{-1}) and November 2005 (Gd_{anth} =137±1 pmol.kg^{-1}) as shown in Figure 10a (Kulaksız and Bau 2007).

In a third scenario (Figure 9c), two distinct freshwater sources with different Gd_{anth} concentrations are mixed with seawater, this can lead in two distinct Gd_{anth} vs Salinity behavior within the same area. It is the case for the San Francisco Bay study by Hatje et al. (2016). Indeed, by representing the concentrations of Gd_{anth} using their dataset (Figure 10b), it is possible to observe two distinct freshwater/seawater conservative mixing patterns. In the northern part of the Bay, by extrapolating Gd_{anth} to part the 0 salinity we obtain 35.1±2.5 pmol.kg^{-1}, which is likely to represent Sacramento River Gd_{anth} concentration at the time of sampling. On the other hand, in the southern part of the Bay, we estimate a substantially higher freshwater source of Gd_{anth} (853 ± 83 pmol.kg^{-1}). This higher level shall correspond to the contribution of WWTP, as four cities located around the southern part of the Bay contributes with WWTP discharges (Palo Alto, San José, Redwood and San Leandro).

Finally, the conservative behavior of Gd_{anth} during estuarine freshwater/seawater mixing can help us identify sources and fate of wastewater and its compounds. The recent study by Andrade et al. (2020) in the Todos os Santos Bay of Salvador showed minor to negligible Gd_{anth} values within the bay except in its eastern portion where a 12h time station was made (Figure 10c). Two relations between Gd_{anth} and salinity appear: from the high to the low tide, the white diamonds indicate a freshwater endmember with highly concentrated Gd_{anth} values of 350 ± 46 pmol.kg^{-1}. In contrast, during the rising tide, a mixing between salty and Gd_{anth} rich waters occurs (black triangles). It is likely that these salty Gd_{anth}-rich waters were originated outside the bay by mixing of waste water from the outfalls of Salvador (located outside the bay, near its entrance) with Atlantic waters. If we perform a mass balance using Pedreira et al. (2018) data for the marine endmember (S=36.8) and WWTP Gd_{anth} concentrations (900-2600 pmol.kg^{-1}), waters having 36.15 ± 0.3 salinity and 25 ± 6 pmol.kg^{-1} of Gd_{anth}

(i.e. waters containing 1-2% waste waters) entered the bay to mix with fresher inner bay waters.

Figure 10 – Anthropogenic gadolinium (Gd_{anth}) in: a) the Weser estuary (Kulaksız and Bau 2007); b) the San Francisco Bay (Hatje et al. 2016) and c) the Todos os Santos Bay (Andrade et al. 2020)
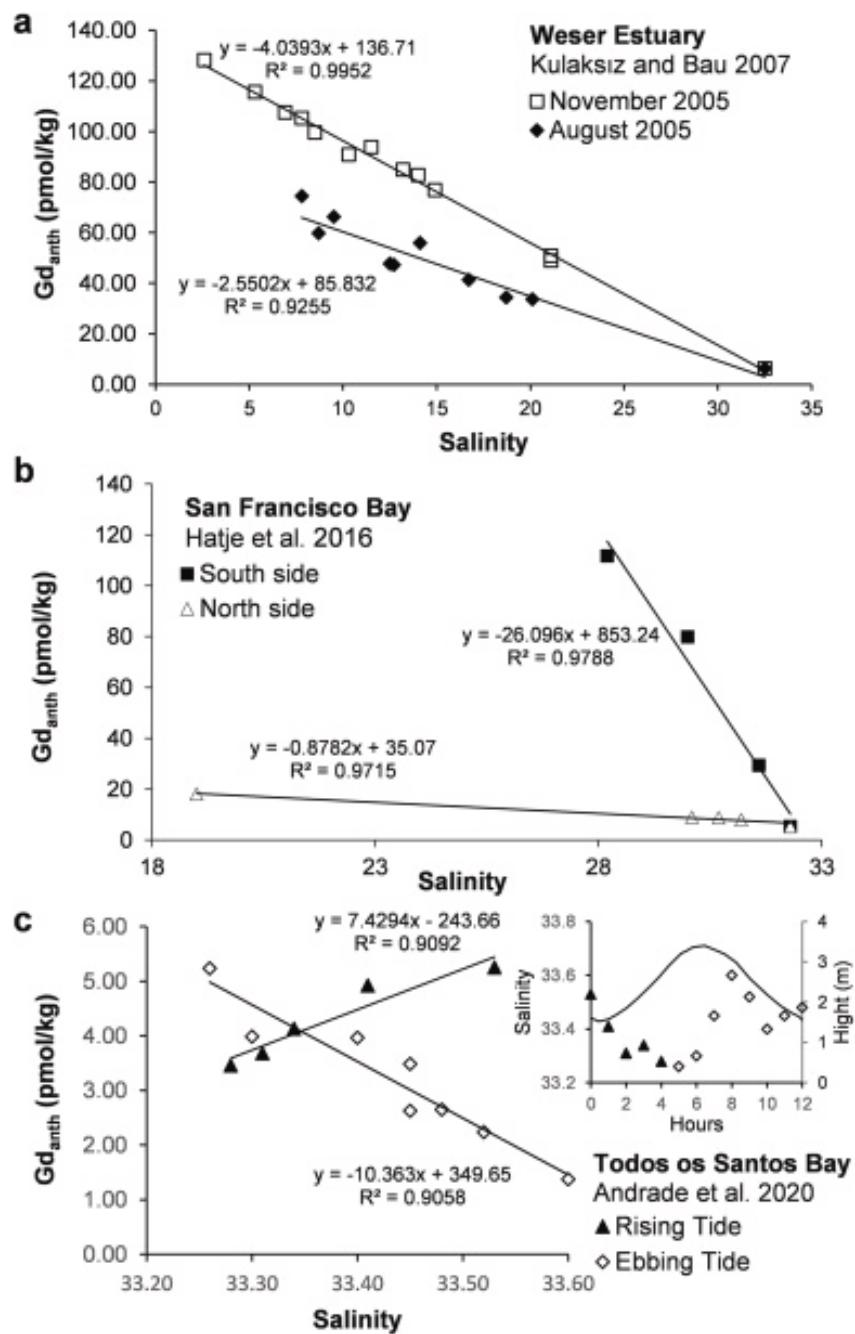
4.1.6 Conclusions

We observed positive Gd anomalies at the WWTP submarine outfall of the city of Fortaleza. This excess of Gd has an anthropogenic origin and is mostly associated with renal excretion of chelated Gd used as a contrasting agent in magnetic resonance imaging. We calculated the absolute concentration of Gd_{anth} and, considering its conservative behavior, we estimated that wastewaters from the WWTP have a Gd_{anth} concentration of 2.2 ± 0.5 nmol.kg^{-1} and delivers annually approximately 25 kg of Gd to the Atlantic Ocean. This load represents roughly half of city's total Gd disposal since the submarine outfall transports 49.1% of Fortaleza wastewaters. A large part of the other half of the Gd disposal reaches two rivers which receive wastewater discharges from the city of Fortaleza and diluting Gd prior to the freshwater/seawater mixing. Using a simple mass balance, we observed that Gd_{anth} is a suitable tool to trace and monitor wastewaters dynamics and dilution in Fortaleza, being potentially helpful for decision and policies making in water management. Further studies are however necessary for such purpose in order to refine the quantitative estimates of source concentration and hydrological variability and thoroughly calibrate this tracer. Moreover, one can infer that the number of MRI analyses have been drastically reduced worldwide during the COVID-19 Pandemic Regarding conservative contaminants, sewage shall present substantially higher threats to biota if launched in river and estuaries than by submarine outfalls as even if diluted, they show higher spatial confinement, longer residence time and higher absolute levels in estuaries. The conservative behavior of both salinity and Gdanth allowed us to classify the mixing of urban water/seawater in three distinct scenarios, this systematic shall be useful for applications in several other coastal cities and estuaries with upstream anthropic impact Increasing the monitoring of this contaminant of emerging concern is important as MRI analyses are facing a constant grow, and little is known regarding its toxicity and the processes that may act as a sink for Gdanth. Finally, this tracer could also be applied as a forensic tool to monitor anthropogenic contamination of source and groundwater polluted by leaking of raw sewage pipes or to detect clandestine wastewater connections to storm sewers in Brazilian cities.

4.1.7 Acknowledgments

4.1.8 Supplementary data

Figure S1 – PAAS normalized Rare Earth elements patterns of sample 6, sample 10 (this study) and AM3 90m (Rousseau et al., 2015)
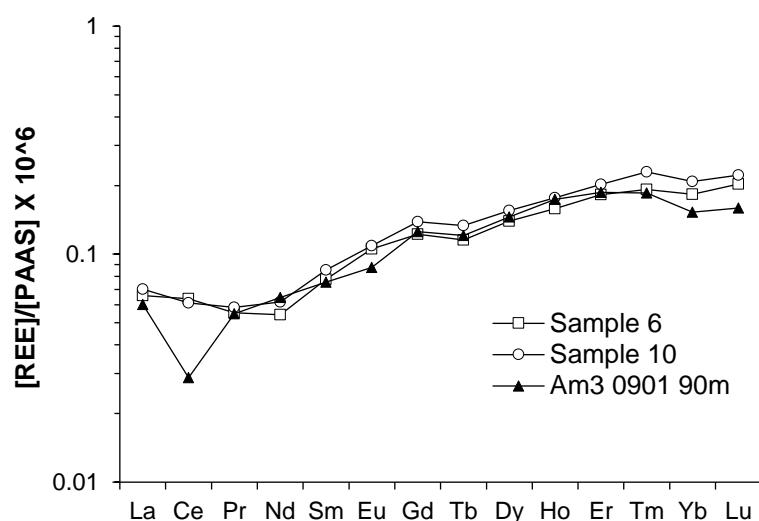
Figure S2 – PAAS normalized Rare Earth Element pattern of sample 11S and its associated third order polynomial fit. The elements represented in orange are used for the regression, the blank space at REE number 5 relates to Pm and the blue triangle is the estimated value for the natural Gd
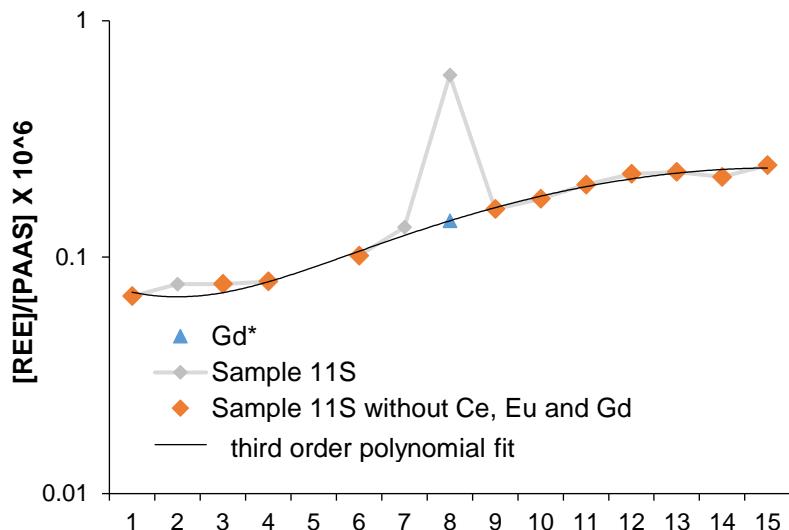
Figure S3 – Sensitivity test of 50% range variation in La values on: a) the shape of the third order polynomial fit b) the variation of Gd* estimated using the fitted polynomial
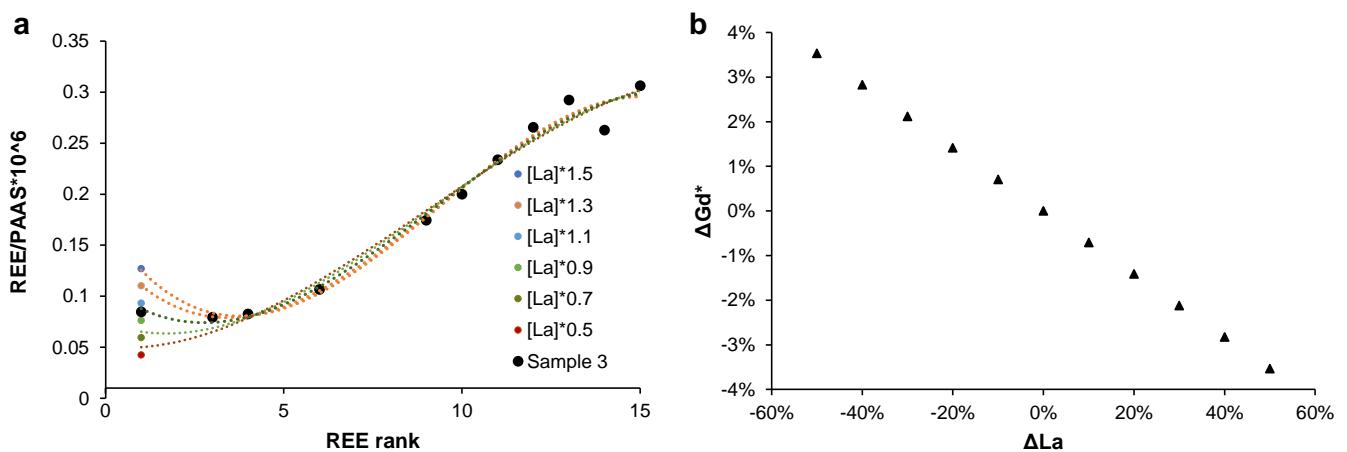
Figure S4 – Anthropogenic Gadolinium (Gd$_{anth}$) as function of salinity in Cocó river (a) and Ceará river (b) estuaries
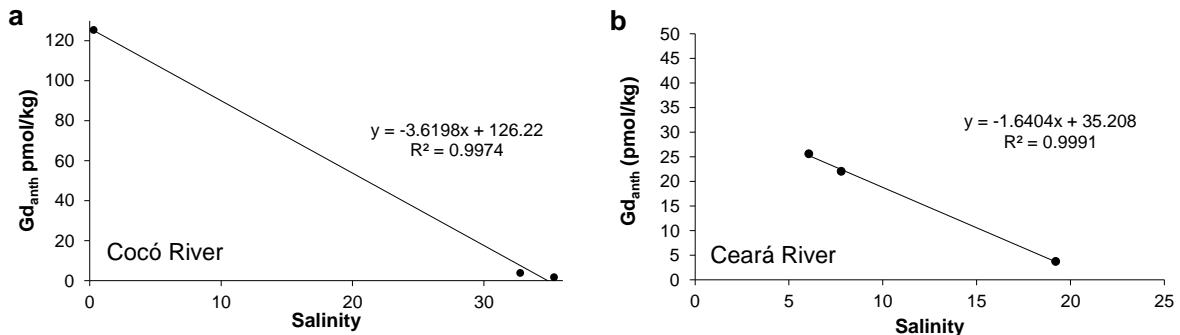
4.1.9 References

Amorim AM, Sodré FF, Rousseau TCC, Maia PD (2019) Assessing rare-earth elements and anthropogenic gadolinium in water samples from an urban artificial lake and its tributaries in the Brazilian Federal District. Microchem J 148:. https://doi.org/10.1016/j.microc.2019.04.055

ANA (2017) Atlas esgotos : despoluição de bacias hidrográficas / Agência Nacional de Águas, Secretaria Nacional de Saneamento Ambiental . -- Brasília: ANA, . Andrade RLB, Hatje V, Pedreira RMA, et al (2020) REE fractionation and human Gd footprint along the continuum between Paraguaçu River to coastal South Atlantic Waters. Chem Geol 119303

Bau M, Dulski P (1996) Anthropogenic origin of positive gadolinium anomalies in river waters. Earth Planet Sci Lett 143:245–255

Bau M, Knappe A, Dulski P (2006) Anthropogenic gadolinium as a micropollutant in river waters in Pennsylvania and in Lake Erie, northeastern United States. Chemie der erde-Geochemistry 66:143–152

CAGECE (2014) Diagnóstico do Sistema de Esgotamento Sanitário

Coppin F, Berger G, Bauer A, et al (2002) Sorption of lanthanides on smectite and kaolinite. Chem Geol 182:57–68

Datasus (2019) Cadastramento Nacional de Estabelecimentos de Saúde – CNES. Relatórios-Equipamentos - Ministerio da saúde. http://cnes2.datasus.gov.br. Accessed 23 Nov 2019

de Campos FF, Enzweiler J (2016) Anthropogenic gadolinium anomalies and rare earth elements in the water of Atibaia River and Anhumas Creek, Southeast Brazil. Environ Monit Assess 188:281

Elderfield H (1988) The oceanic chemistry of the rare-earth elements. Philos Trans R

Soc London Ser A, Math Phys Sci 325:105–126

Feng X, Xia Q, Yuan L, et al (2010) Impaired mitochondrial function and oxidative stress in rat cortical neurons: implications for gadolinium-induced neurotoxicity. Neurotoxicology 31:391–398

Ferreira AG, da Silva Mello NG (2005) Principais sistemas atmosféricos atuantes sobre a região Nordeste do Brasil e a influência dos oceanos Pacífico e Atlântico no clima da região. Rev Bras Climatol 1:

Fujita Y, Walton M, Das G, et al (2020) Impacts of anthropogenic gadolinium on the activity of the ammonia oxidizing bacterium Nitrosomonas europaea. Chemosphere 127250

Garcia-Solsona E, Jeandel C, Labatut M, et al (2014) Rare earth elements and Nd isotopes tracing water mass mixing and particle-seawater interactions in the SE Atlantic. Geochim Cosmochim Acta 125:351–372

Hatje V, Bruland KW, Flegal AR (2016) Increases in anthropogenic gadolinium anomalies and rare earth element concentrations in San Francisco Bay over a 20 year record. Environ Sci Technol 50:4159–4168

Henderson P (1984) General geochemical properties and abundances of the rare earth elements. In: Developments in geochemistry. Elsevier, pp 1–32

Henriques B, Coppola F, Monteiro R, et al (2019) Toxicological assessment of anthropogenic Gadolinium in seawater: Biochemical effects in mussels Mytilus galloprovincialis. Sci Total Environ 664:626–634

IBGE (2019) Informações gerais sobre Fortaleza. https://www.ibge.gov.br/cidades-e-estados/ce/fortaleza.html. Accessed 15 Dec 2019

INMET (2019) Normais climatológicas do Brasil. http://www.inmet.gov.br/. Accessed 15 Dec 2019

Johannesson KH, Palmore CD, Fackrell J, et al (2017) Rare earth element behavior during groundwater–seawater mixing along the Kona Coast of Hawaii. Geochim Cosmochim Acta 198:229–258

Klaver G, Verheul M, Bakker I, et al (2014) Anthropogenic Rare Earth Element in rivers: Gadolinium and lanthanum. Partitioning between the dissolved and particulate phases in the Rhine River and spatial propagation through the Rhine-Meuse Delta (the Netherlands). Appl Geochemistry 47:186–197

Köhler SJ, Harouiya N, Chaïrat C, Oelkers EH (2005) Experimental studies of REE fractionation during water–mineral interactions: REE release rates during apatite dissolution from pH 2.8 to 9.2. Chem Geol 222:168–182

Kulaksız S, Bau M (2007) Contrasting behaviour of anthropogenic gadolinium and natural rare earth elements in estuaries and the gadolinium input into the North Sea.

Earth Planet Sci Lett 260:361–371. https://doi.org/https://doi.org/10.1016/j.epsl.2007.06.016

Kulaksız S, Bau M (2011) Rare earth elements in the Rhine River, Germany: first case of anthropogenic lanthanum as a dissolved microcontaminant in the hydrosphere. Environ Int 37:973–979

Kümmerer K, Helmers E (2000) Hospital effluents as a source of gadolinium in the aquatic environment. Environ Sci Technol 34:573–577

Lawrence MG (2010) Detection of anthropogenic gadolinium in the Brisbane River plume in Moreton Bay, Queensland, Australia. Mar Pollut Bull 60:1113–1116

Lerat-Hardy A, Coynel A, Dutruch L, et al (2019) Rare Earth Element fluxes over 15 years into a major European Estuary (Garonne-Gironde, SW France): Hospital effluents as a source of increasing gadolinium anomalies. Sci Total Environ 656:409–420

Luo Y-R, Byrne RH (2004) Carbonate complexation of yttrium and the rare earth elements in natural waters. Geochim Cosmochim Acta 68:691–699

McLennan SMSM (1989) Rare earth elements in sedimentary rocks: influence of provenance and sedimentary processes. Geochemistry Mineral Rare Earth Elem Rev Mineral 21 21:169–200

Merschel G, Bau M, Baldewein L, et al (2015) Tracing and tracking wastewater-derived substances in freshwater lakes and reservoirs: Anthropogenic gadolinium and geogenic REEs in Lake Paranoá, Brasilia. Comptes Rendus Geosci 347:284–293. https://doi.org/https://doi.org/10.1016/j.crte.2015.01.004

Möller P, Dulski P, Bau M, et al (2000) Anthropogenic gadolinium as a conservative tracer in hydrology. J Geochemical Explor 69:409–414

Möller P, Paces T, Dulski P, Morteani G (2002) Anthropogenic Gd in surface water, drainage system, and the water supply of the city of Prague, Czech Republic. Environ Sci Technol 36:2387–2394

Mortatti BC, Enzweiler J (2019) Major ions and rare earth elements hydrogeochemistry of the Atibaia and Jaguari rivers subbasins (Southeast Brazil). Appl Geochemistry 111:104461

Nilin J, Moreira LB, Aguiar JE, et al (2013) Sediment quality assessment in a tropical estuary: the case of Ceará River, Northeastern Brazil. Mar Environ Res 91:89–96

Nozaki Y, Lerche D, Alibo DS, Tsutsumi M (2000) Dissolved indium and rare earth elements in three Japanese rivers and Tokyo Bay: evidence for anthropogenic Gd and In. Geochim Cosmochim Acta 64:3975–3982

OECD (2020) Magnetic resonance imaging (MRI) units. https://data.oecd.org/healtheqt/magnetic-resonance-imaging-mri-units.htm. Accessed

29 Apr 2020

Oksendal AN, Hals P (1993) Biodistribution and toxicity of MR imaging contrast media. J Magn Reson Imaging 3:157–165

Pałasz A, Czekaj P (2000) Toxicological and cytophysiological aspects of lanthanides action. Acta Biochim Pol 47:1107–1114

Pedreira RMA, Pahnke K, Böning P, Hatje V (2018) Tracking hospital effluent-derived gadolinium in Atlantic coastal waters off Brazil. Water Res 145:62–72

Pereira SP, Rosman PCC, Alvarez C, et al (2015) Modeling of coastal water contamination in Fortaleza (Northeastern Brazil). Water Sci Technol 72:928–936

Rabiet M, Letouzet M, Hassanzadeh S, Simon S (2014) Transmetallation of Gd-DTPA by Fe3+, Cu2+ and Zn2+ in water: Batch experiments and coagulation–flocculation simulations. Chemosphere 95:639–642

Rousseau TCC, Sonke JE, Chmeleff J, et al (2015) Rapid neodymium release to marine waters from lithogenic sediments in the Amazon estuary. Nat Commun 6:. https://doi.org/10.1038/ncomms8592

Rousseau TCC, Sonke JE, Chmeleff J, et al (2013) Rare earth element analysis in natural waters by multiple isotope dilution-sector field ICP-MS. J Anal At Spectrom 28:. https://doi.org/10.1039/c3ja30332b

Schijf J, Christy IJ (2018) Effect of Mg and Ca on the stability of the MRI contrast agent Gd–DTPA in seawater. Front Mar Sci 5:111

Schmidt K, Bau M, Merschel G, Tepe N (2019) Anthropogenic gadolinium in tap water and in tap water-based beverages from fast-food franchises in six major cities in Germany. Sci Total Environ 687:1401–1408

Shabani MB, Akagi T, Masuda A (1992) Preconcentration of trace rare-earth elements in seawater by complexation with bis (2-ethylhexyl) hydrogen phosphate and 2-ethylhexyl dihydrogen phosphate adsorbed on a C18 cartridge and determination by inductively coupled plasma mass spectrometry. Anal Chem 64:737–743

Shellock FG (2000) Magnetic resonance procedures: health effects and safety. Crc Press

Sholkovitz ER (1993) The geochemistry of rare earth elements in the Amazon River estuary. Geochim Cosmochim Acta 57:2181–2190

Sholkovitz ER, Landing WM, Lewis BL (1994) Ocean particle chemistry: the fractionation of rare earth elements between suspended particles and seawater. Geochim Cosmochim Acta 58:1567–1579

Telgmann L, Sperling M, Karst U (2013) Determination of gadolinium-based MRI contrast agents in biological and environmental samples: a review. Anal Chim Acta

764:1–16

Tepe N, Romero M, Bau M (2014) High-technology metals as emerging contaminants: Strong increase of anthropogenic gadolinium levels in tap water of Berlin, Germany, from 2009 to 2012. Appl Geochemistry 45:191–197

Xia Q, Feng X, Huang H, et al (2011) Gadolinium-induced oxidative stress triggers endoplasmic reticulum stress in rat cortical neurons. J Neurochem 117:38–47

Yeghicheyan D, Aubert D, Bouhnik-Le Coz M, et al (2019) A New Interlaboratory Characterisation of Silicon, Rare Earth Elements and Twenty-Two Other Trace Element Concentrations in the Natural River Water Certified Reference Material SLRS-6 (NRC-CNRC). Geostand Geoanalytical Res 43:475–496

Zhou Z, Lu Z (2013) Gadolinium-based contrast agents for magnetic resonance cancer imaging. Wiley Interdiscip Rev Nanomedicine Nanobiotechnology 5:1–18

4.2 Elementos Terras-Raras dissolvidos no Delta do Parnaíba

Artigo em preparação.

4.2.1 Introdução

A foz do rio Parnaíba é composta por um sistema deltaico que cobre uma área de 270.000 hectares. O Delta do rio Parnaíba é o único delta de mar aberto das Américas e é o foco deste estudo. Em 1996 passou a integrar uma Área de Proteção Ambiental (APA) que abrange os estados do Maranhão, Ceará e Piauí, e percorre todo litoral deste último. Em 2000 foi criada a Reserva Extrativista (RESEX) Delta do Parnaíba que possui uma área de aproximadamente 27.022 hectares e está inserida na APA Delta do Parnaíba (LACERDA, 2018; MINISTÉRIO DO MEIO AMBIENTE, 2006).

O Delta do Parnaíba é marcado pela presença de baías, canais de maré com características estuarinas e inúmeras ilhas de mangue. As espécies de mangue dominantes são *Rhizophora mangle, Avicennia germinans* e *Laguncularia racemosa.* As árvores podem atingir mais de 20 metros de altura e a extensão das florestas de mangue, por sua vez, pode atingir mais de 150.000 ha. O delta também possui amplos campos de dunas móveis que já avançam sobre o mangue no setor leste (LACERDA, 2018). Além disso, o complexo deltaico da foz do rio Parnaíba abriga importantes comunidades animais e merece atenção especial para a sua conservação (MINISTÉRIO DO MEIO AMBIENTE, 2006).

As características geomorfológicas indicam que o Delta do Parnaíba é assimétrico e dominado por ondas e marés. O rio Parnaíba é o maior fornecedor de sedimentos para o Delta (AQUINO DA SILVA et al., 2015a, 2019). Aquino da Silva et al. (2015b) verificaram que apesar da relação entre a precipitação e a concentração de sedimentos em suspensão não ser linear, a primeira é o principal fator que influencia a sazonalidade da segunda no rio Parnaíba.

O Delta do Parnaíba possui uma ampla zona estuarina marcada pelo fluxo significativo de sedimentos para a costa e presença de mangues densos, baías e campos de dunas. Por sua extensão e diversidade de ambientes esta região deve ter papel significante na transferência de materiais na interface continente-oceano. Porém, apesar da importância geoquímica, o Delta ainda é pouco estudado.

Os Elementos Terras-Raras (ETRs) são um grupo de elementos com propriedades químicas muito próximas devido ao preenchimento gradual da camada de elétrons 4f. Isso leva a uma diminuição do raio iônico conforme aumento do número atômico que é denominada de contração dos lantanídeos (HENDERSON, 1983). Essas características ocasionam uma variação gradual de reatividade desses elementos em processos geoquímicos. E isso permite que eles sejam utilizados como traçadores eficientes desses processos em diversos ambientes como rios e estuários (GAILLARDET; VIERS; DUPRÉ, 2003; SHOLKOVITZ, 1995).

Os ETRs, no entanto, são traços em ambientes aquáticos apresentando concentrações na ordem de parte por trilhão (ppt) e por isso o emprego de métodos de extração se fazem necessários. A pré-concentração dos Elementos Terras-Raras tem sido realizada por meio de extração em fase sólida, seguindo protocolo adaptado de Shabani; Akagi; Masuda (1992), Merschel et al. (2015), Amorim et al. (2019) e Da Costa et al. (2021).

Este estudo inédito dos Elementos Terras-Raras em águas superficiais do Delta do Parnaíba deverá contribuir para a caracterização dos processos controladores da distribuição geoquímica desses elementos na fase dissolvida, além da verificação da influência das diferentes fontes de ETRs na região.

4.2.2 Material e Métodos

4.2.2.1 Área de estudo

O clima na região do Delta do rio Parnaíba sofre influência da Zona de Convergência Intertropical (ZCIT) e das Linhas de Instabilidade Tropical (LIT) oriundas da Amazônia Oriental. Além disso, os fenômenos El Niño e La Niña são responsáveis por mudanças nas condições climáticas, provocando diminuição ou aumento nos totais de chuva, respectivamente (MINISTÉRIO DO MEIO AMBIENTE, 2006). O regime pluviométrico é caracterizado por uma estação chuvosa que dura de janeiro a maio e uma estação seca que ocorre de junho a dezembro (AQUINO DA SILVA et al., 2015a).

A maré é semidiurna e atinge amplitudes de 3.06 e 1.7 metros durante a preamar de sizígia e de quadratura, respectivamente. Os ventos predominantes na região são os alísios de NE. As ondas apresentam a direção SW como dominante e

junto a ação dos ventos produzem uma corrente longitudinal leste-oeste. Em sua parte oeste o Delta do rio Parnaíba possui um sistema de canal de maré que é conectado ao canal principal/rio Parnaíba por meio de um canal artificial aberto na década de 1960 (AQUINO DA SILVA et al., 2015a) e ativo até hoje, por onde navegam barcos de médio porte.

Na costa os sedimentos provenientes do rio Parnaíba são transportados e distribuídos pela corrente de deriva litorânea, fazendo com que os sedimentos finos existentes nos canais de maré no lado ocidental do Delta sejam oriundos da pluma do rio Parnaíba. Esse fluxo de sedimentos para a costa contribui para a estabilidade da mesma na região do Delta do rio Parnaíba. Mas além disso, fatores como a pouca ocupação humana e a interferência mínima ao longo do curso do rio também contribuem para que a linha de costa nessa região seja estável (AQUINO DA SILVA et al., 2019).

Os sedimentos do sistema deltaico do rio Parnaíba ainda não apresentam concentrações de metais pesados em níveis que indiquem contaminação (DE PAULA FILHO et al., 2015). Além disso, insumos urbanos oferecem pouca contribuição na emissão de nitrogênio (N) e fósforo (P) para a região. Porém, as atividades humanas tipicamente rurais como agricultura, pecuária e carcinicultura, já se mostram ser uma importante fonte antrópica de N e P para o estuário do rio Parnaíba (DE PAULA FILHO; MARINS; DE LACERDA, 2015).

Quanto a hidroquímica, no canal principal/Rio Parnaíba durante a estação seca é possível verificar a formação de gradiente de salinidade, apesar de restrito a região mais externa onde o rio se conecta com o mar. Porém, com o aumento do fluxo fluvial durante a estação chuvosa todo o canal passa a apresentar salinidade de valor zero. O pH também muda entre as estações, variando de 7.2 a 7.9 na seca e de 7.4 a 8.5 na chuvosa (PAULA FILHO et al., 2020).

A Bacia Hidrográfica do Parnaíba drena 223 municípios piauienses, 35 maranhenses e 19 cearenses, e tem cerca de 5 milhões de habitantes (AGÊNCIA NACIONAL DE ÁGUAS E SANEMENTO BÁSICO, 2020). Há poucas informações sobre a qualidade das águas superficiais da bacia, mas o maior problema enfrentado é o lançamento de esgoto *in natura* nos corpos hídricos. Isso ocorre, por exemplo, na área de maior contingente populacional onde ficam localizadas as cidades de Teresina-PI e Timon-MA distantes aproximadamente 270km do Delta, onde vivem quase 1 milhão de habitantes e a água é utilizada para despejo de esgotos sanitários.

A carga poluidora doméstica lançada na região hidrográfica é estimada em 122 t DBO$_{5,20}$/dia (AGÊNCIA NACIONAL DE ÁGUAS, 2005; MINISTÉRIO DO MEIO AMBIENTE, 2006).

4.2.2.2 Amostragem

A malha amostral consistiu em 18 pontos, 3 dos quais localizados no canal principal e o restante distribuídos nos canais de maré e nas baías no lado Oeste do Delta (Fig. 11). A tabela 3 contém as coordenadas de cada ponto, a data da coleta e dados hidroquímicos, os quais salinidade e temperatura foram medidos com sonda multiparamétrica portátil YSI (modelo professional plus), e pH com pHmetro portátil (Metrohm). Em todos os pontos foram coletadas amostras de água superficial com garrafas de polietileno de alta densidade (PEAD) de 1L. Essas amostras foram filtradas com filtros de acetato de celulose de 0,45 μm usando suportes de filtros de policarbonato (Millipore), logo após a coleta e estocadas para posterior pré-concentração e determinação dos ETRs em laboratório.

Tabela 3 – Localização e dados hidroquímicos dos pontos amostrais

Ponto	Latitude S	Longitude W	Salinidade	T (°C)	pH	Data
1	2° 50,145	41° 51,081	0	29.7	7.41	13/12/2020
2	2° 46,969	41° 50,834	17.4	29.5	8.04	13/12/2020
3	2° 45,445	41° 49,417	36.2	29.3	8.1	13/12/2020
4	2° 50,3618	41° 53,9584	2.3	29.2	6.78	12/12/2020
5	2° 49,6905	41° 54,0491	0.5	-	-	13/12/2020
6	2° 49,2971	41° 54,4421	1.6	-	-	13/12/2020
7	2° 48,9739	41° 54,5777	2.4	-	-	13/12/2020
8	2° 48,1734	41° 54,4187	6.4	-	-	13/12/2020
9	2° 47,794	41° 55,484	11.7	29.6	6.98	12/12/2020
10	2° 48,3709	41° 56,6338	20.1	-	-	13/12/2020
11	2° 48,3330	41° 56,8433	15.3	29.9	7.18	12/12/2020
12	2° 48,1712	41° 57,1725	23.8	-	-	13/12/2020
13	2° 46,0590	41° 59,8672	34.7	29.1	8.02	12/12/2020
14	2° 45,084	42° 00,907	35	29.5	8.12	12/12/2020
15	2° 48,095	42° 04,142	33.3	29.6	7.71	13/12/2020
16	2° 46,583	42° 05,017	35.07	29.4	7.99	12/12/2020
17	2° 44,4388	42° 7,1931	36.3	29	8.06	13/12/2020
18	2° 43,950	42° 15,929	36.5	29.2	8.09	13/12/2020

Figura 11 – Mapa amostral
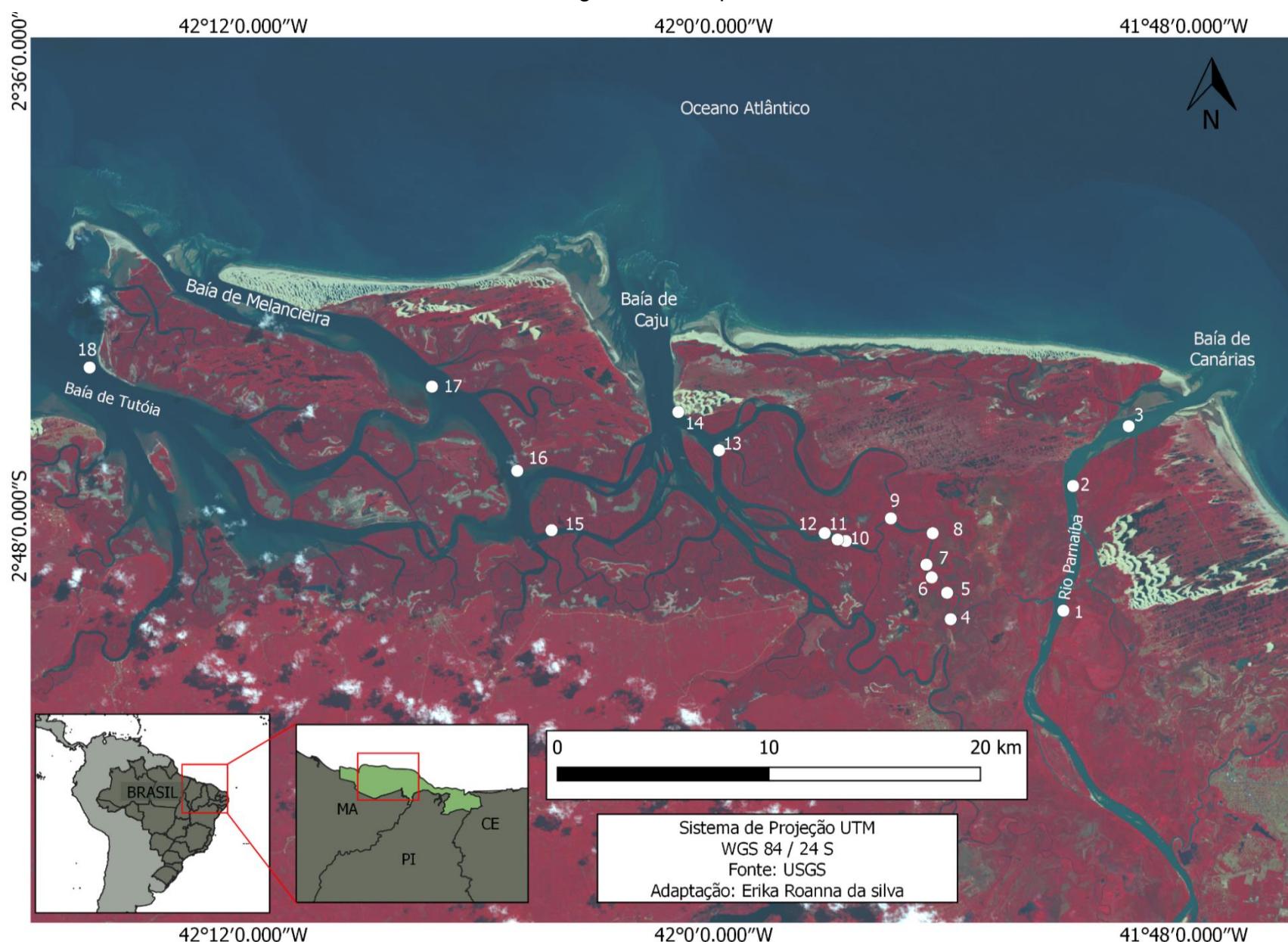
4.2.2.3 Procedimentos analíticos

Em laboratório, todas as amostras foram acidificadas até um pH próximo a 2. Isso garante que os metais nas amostras fiquem na forma dissolvida evitando adsorção na parede do frasco, além de uma boa recuperação no procedimento de pré-concentração (BAU; DULSKI, 1996). Após a acidificação, foi adicionada às amostras uma mistura de *spike* enriquecida nos isótopos ^{146}Nd, ^{151}Eu e ^{172}Yb (DA COSTA et al., 2021; ROUSSEAU et al., 2013).

Ácidos clorídrico (Merck, PA) e nítrico (Merck) utilizados na pré-concentração e na limpeza do material foram bidestilados em destilador de Quartz e posteriormente padronizados. As garrafas PEAD, utilizadas para a estocagem das amostras, foram limpas com HCl 0,5M (NEON, PA). Filtros de acetato de celulose de 0,45 μm e suportes de policarbonato (Millipore) foram limpos em banho de HNO_3 bidestilado 0,35M e com HCl 0,35M, respectivamente. Além disso, água Milli-Q foi utilizada em todos os procedimentos.

Os cartuchos C18 (Waters, Sep-Pak) utilizados para a pré-concentração foram limpos passando-se 20 mL de HCl 2M a uma vazão de cerca de 3,4 mL/min. Os cartuchos ficaram, então, 24 horas em banho de HCl 2M e foram limpos passando-se 100 mL de água Milli-Q a uma vazão de cerca de 8,5 mL/min. Após essa limpeza inicial, os cartuchos foram carregados aspirando-se com uma seringa o agente complexante fosfato de 2-etilhexilo (HDMEP-H_2DMEP) até cerca de dois terços de cada cartucho e limpos com 10 mL de HCl 6M em uma vazão de cerca de 3,4 mL/min. e com 40 mL de água Milli-Q em uma vazão de cerca de 8,5 mL/min.

As amostras foram pré-concentradas passando-se as mesmas através dos cartuchos C18 previamente tratados, a uma vazão média de cerca de 9,8 mL/min. Antes da eluição dos ETRs passou-se pelos cartuchos 10 mL de HCl 0,01M a uma vazão média de cerca de 3,3 mL/min para retirada do Ba interferente e a eluição final dos ETRs foi feita usando-se 40 mL de HCl 6M, a uma vazão de 3,3 mL/min.

O produto da eluição de cada amostra foi recolhido em tubos de Teflon que foram aquecidos a cerca de 160 °C para a evaporação total do HCl 6M. Após a evaporação, dissolveu-se os resíduos com 5 mL de HNO_3 0,32M que se tornou a matriz final.

As análises dos ETRs foram realizadas em um espectrômetro de massa com plasma indutivamente acoplado (ICPMS) quadrupolo iCAP RQ (Thermo). As

concentrações dos ETRs foram obtidas por diluição isotópica a partir da mistura de *spike* adicionada às amostras antes da pré-concentração e por calibração externa de um ponto.

4.2.3 Resultados

A salinidade (Tabela 3) variou de 0 a 36.2 no canal principal e de 0.5 a 36.5 no lado Oeste do Delta. A temperatura variou de 29 a 29.9 °C (Tabela 3). A variação do pH (Tabela 3) foi de 7.41 a 8.10 para o canal principal e de 6.78 a 8.12 para o lado Oeste.

A tabela 4 apresenta as concentrações e o somatório das concentrações dos ETRs. As maiores concentrações dos Elementos Terras-Raras do estudo foram observadas para o ponto zero de salinidade (Ponto 1) com ∑ETRs 3417.4 pmol/kg, seguido do ponto 0.5 de salinidade (Ponto 5) com ∑ETRs 2906.4 pmol/kg e do ponto 2.3 de salinidade (Ponto 4) com ∑ETRs 1679.5 pmol/kg. Já as menores concentrações foram para o Ponto 8 com salinidade 6.4 e ∑ETRs 156.4 pmol/kg.

Tabela 4 – Concentrações dos ETRs na fração dissolvida, em pmol/kg

Amostra	La	Ce	Pr	Nd	Sm	Eu	Gd	Tb	Dy	Ho	Er	Tm	Yb	Lu	∑ETR
1	604.4	1335.2	185.3	737.2	152.8	34.7	139.5	18.8	97.9	18.6	47.6	5.9	34.6	4.9	3417.4
2	128.3	91.2	22.3	98.5	19.8	5.4	29.0	4.4	28.6	7.4	21.8	2.8	15.9	2.5	478.0
3	94.7	84.5	23.3	101.1	22.6	6.2	32.1	5.0	33.8	8.3	24.9	3.3	18.9	2.9	461.6
4	289.4	668.9	83.3	349.7	73.4	17.2	68.1	9.3	52.4	10.2	28.5	3.7	22.0	3.4	1679.5
5	486.5	1182.2	147.3	616.4	125.9	28.0	117.5	15.8	84.6	16.3	43.5	5.6	32.2	4.6	2906.4
6	46.0	57.6	12.8	60.7	14.8	4.0	18.1	2.4	15.0	3.2	9.6	1.3	8.2	1.4	255.3
7	39.2	39.9	9.1	43.2	10.4	3.2	13.7	1.7	11.7	2.6	8.2	1.1	7.0	1.1	192.0
8	41.5	27.9	6.8	31.9	7.5	2.4	10.6	1.4	9.6	2.2	6.7	0.9	5.9	1.0	156.4
9	78.2	37.1	9.0	41.4	8.2	2.3	12.7	1.6	10.8	2.7	8.3	1.1	6.8	1.1	221.4
10	88.3	48.2	11.4	52.8	10.9	3.0	17.0	2.6	17.5	4.3	13.5	1.9	11.0	1.8	284.2
11	81.7	49.5	11.5	51.9	10.4	2.8	15.9	2.1	14.8	3.6	11.3	1.5	9.0	1.4	267.5
12	127.7	141.6	21.1	91.4	19.5	5.3	28.7	4.2	28.6	7.2	21.9	3.0	17.1	2.7	520.0
13	88.3	100.1	18.5	85.1	19.2	5.2	28.4	4.9	32.6	8.2	25.5	3.4	20.3	3.2	443.0
14	88.1	126.2	20.0	88.0	19.1	5.5	27.2	4.2	29.3	7.0	21.9	2.9	16.8	2.7	458.7
15	116.9	150.1	23.2	100.2	21.8	6.3	32.8	5.0	34.9	8.6	26.4	3.5	20.1	3.2	552.8
16	85.6	107.9	18.0	80.5	18.8	5.4	27.9	4.8	32.6	8.2	25.4	3.5	20.8	3.4	442.7
17	63.1	85.6	15.3	66.8	15.6	4.4	23.2	3.7	26.7	6.7	21.0	2.8	16.6	2.6	354.2
18	62.6	84.1	14.3	67.5	15.8	4.5	24.4	4.2	28.8	7.2	22.7	3.1	18.9	3.1	361.4

A variação dos ETRs na fração dissolvida em relação a salinidade (Fig. 12) indica que os teores diminuem no intervalo de 0 a 6.4, seguido de um aumento no intervalo de 11.7 a 33.3 de salinidade. Para o Nd, representante dos *LREE*, a diminuição é de 737.2 pmol/kg para 31.9 pmol/kg e o aumento de 41.4 pmol/kg para 100.2 pmol/kg. Para o Gd, representante dos *MREE*, a diminuição é de 139.5 pmol/kg para 10.6 pmol/kg e o aumento de 12.7 pmol/kg para 32.8 pmol/kg. Finalmente, para o Yb, representante dos *HREE*, a diminuição é de 34.6 pmol/kg para 5.9 pmol/kg e o aumento de 6.8 pmol/kg para 20.1 pmol/kg. Destaque para o Ce que teve as maiores variações com a diminuição de 1335.2 pmol/kg para 27.9 pmol/kg e aumento de 37.1 pmol/kg para 150.1 pmol/kg.

Figura 12 – Dados do lado Oeste do Delta e zero de salinidade
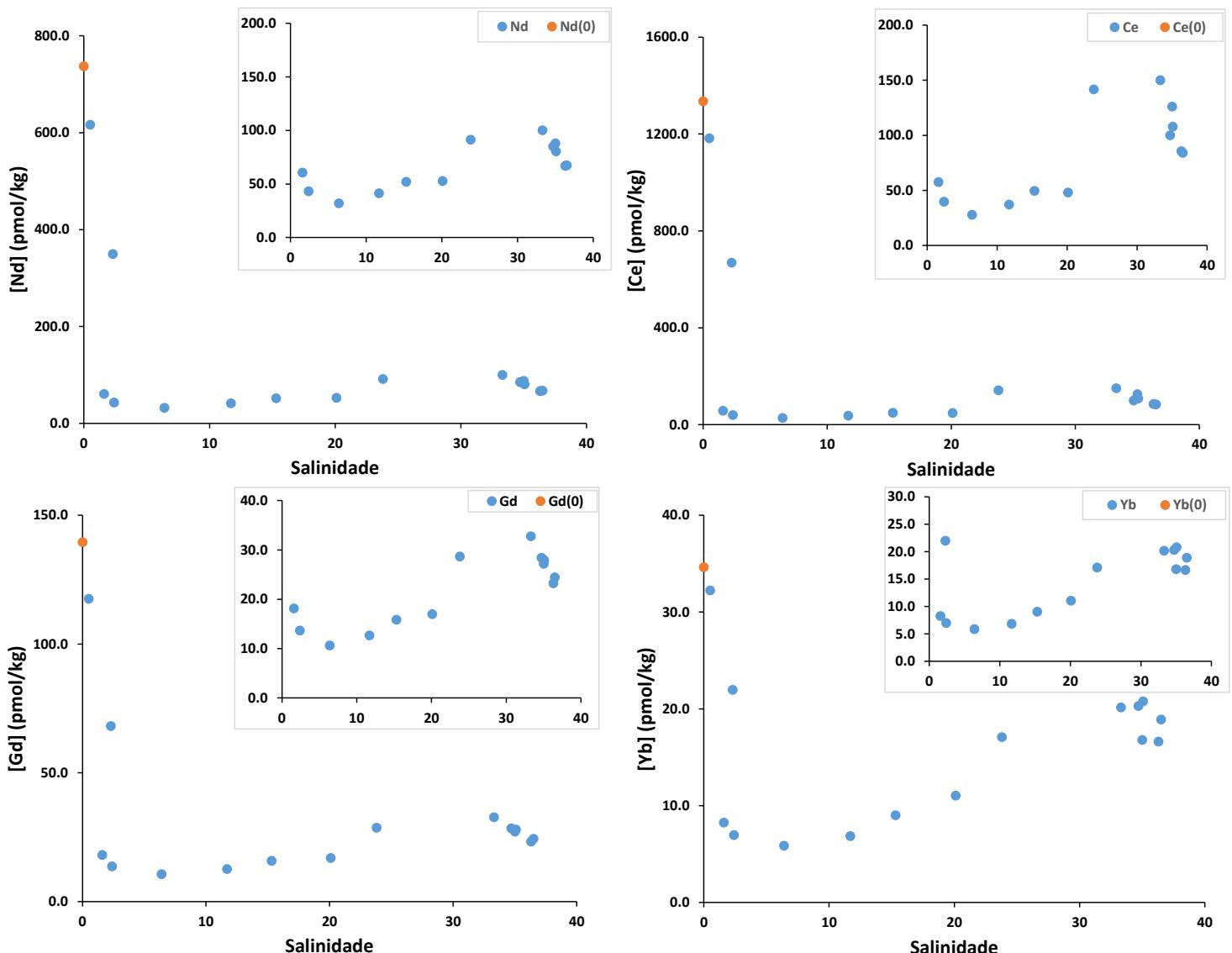
A figura 13 contém os padrões de distribuição dos ETRs. Nenhum padrão apresentou anomalias positivas de gadolínio. No canal principal (Fig. 13a) o padrão de distribuição para o ponto com salinidade zero (Ponto 1) apresentou as maiores concentrações relativas do estudo e um enriquecimento de *MREE*. Já os padrões dos pontos 2 e 3 apresentaram anomalia negativa de Ce e enriquecimento de *HREE*.

Para o lado Oeste do Delta (Fig. 13b), os padrões de distribuição dos ETRs dos pontos 4 e 5 tiveram comportamento semelhante ao ponto 1 do canal principal com enriquecimento de *MREE* e altas concentrações relativas. Já nos padrões de distribuição dos pontos 6 ao 18 é possível observar a presença de anomalias negativas de Ce e enriquecimento de *HREE* que são marcas de águas mais salinas.

Figura 13 – Padrões de distribuição dos ETRs para a) Canal principal e b) Lado Oeste do Delta
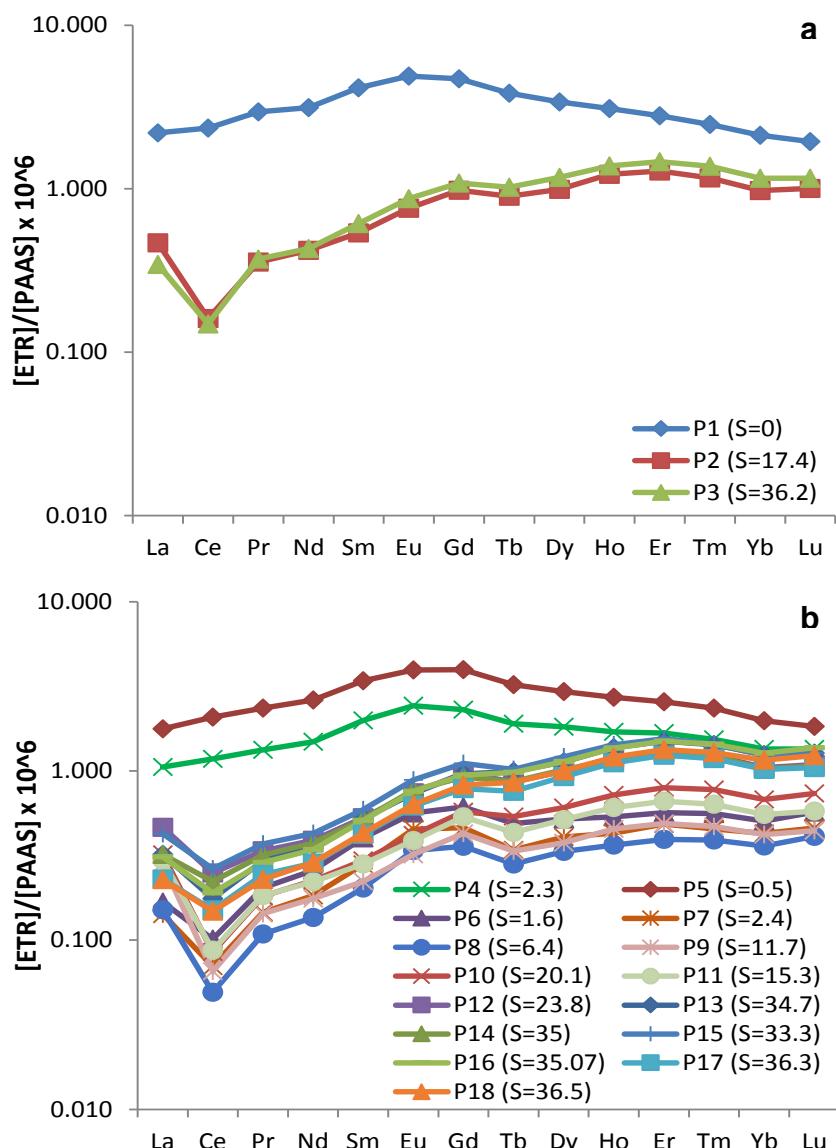
As anomalias de Ce foram calculadas a partir da equação 6 onde Ce* é concentração estimada deste elemento sem anomalia, e Ce_{sn}, La_{sn} e Pr_{sn} são as concentrações de ETRs normalizadas pelo PAAS.

$$Ce/Ce^* = Ce_{sn}/(La_{sn} \times Pr_{sn})^{0.5}$$ Eq. 6

Os maiores valores (0.92, 1.00 e 1.02) foram observados para as amostras de menor salinidade (Pontos 1, 4 e 5) que, portanto, não apresentaram anomalia. Todos os demais pontos, no entanto, apresentaram anomalia negativa deste elemento com valores de Ce/Ce* variando de 0.32 (Ponto 9) a 0.70 (Ponto 14) e com valor médio de 0.52 ± 0.13. Dessa forma, o gradiente estuarino influenciou de modo diferenciado com a remoção do Ce nas amostras mais salinas atestada pela presença de anomalia negativa do mesmo.

4.2.4 Referências

AGÊNCIA NACIONAL DE ÁGUAS. **Panorama da qualidade das águas superficiais no Brasil**. Brasília: ANA, SPR, 2005.

AGÊNCIA NACIONAL DE ÁGUAS E SANEMENTO BÁSICO. **CBH Parnaíba**. Disponível em: <https://www.ana.gov.br/aguas-no-brasil/sistema-de-gerenciamento-de-recursos-hidricos/cbh-parnaiba/cbh-parnaiba-texto>. Acesso em: 14 set. 2020.

AMORIM, A. M. et al. Assessing rare-earth elements and anthropogenic gadolinium in water samples from an urban artificial lake and its tributaries in the Brazilian Federal District. **Microchemical Journal**, v. 148, n. April, p. 27–34, 2019.

AQUINO DA SILVA, A. G. et al. The Influence of Climatic Variations on River Delta Hydrodynamics and Morphodynamics in the Parnaíba Delta, Brazil. **Journal of Coastal Research**, v. 31, n. 4, p. 930–940, 2015a.

AQUINO DA SILVA, A. G. et al. Spectral calibration of CBERS 2B multispectral satellite images to assess suspended sediment concentration. **ISPRS Journal of Photogrammetry and Remote Sensing**, v. 104, p. 53–62, 2015b.

AQUINO DA SILVA, A. G. et al. Coastline change and offshore suspended sediment dynamics in a naturally developing delta (Parnaíba Delta, NE Brazil). **Marine Geology**, v. 410, n. December 2018, p. 1–15, 2019.

BAU, M.; DULSKI, P. Anthropogenic origin of positive gadolinium anomalies in river waters. **Earth and Planetary Science Letters**, v. 143, n. 1–4, p. 245–255, 1996.

DA COSTA, A. R. B. et al. Anthropogenic gadolinium in estuaries and tropical Atlantic coastal waters from Fortaleza, Northeast Brazil. **Applied Geochemistry**, v. 127, n. February, 2021.

DE PAULA FILHO, F. J. et al. Background values for evaluation of heavy metal contamination in sediments in the Parnaíba River Delta estuary, NE/Brazil. **Marine Pollution Bulletin**, v. 91, n. 2, p. 424–428, 2015.

DE PAULA FILHO, F. J.; MARINS, R. V.; DE LACERDA, L. D. Natural and anthropogenic emissions of N and P to the Parnaíba River Delta in NE Brazil. **Estuarine, Coastal and Shelf Science**, v. 166, p. 34–44, 2015.

GAILLARDET, J.; VIERS, J.; DUPRÉ, B. Trace Elements in River Waters. **Treatise on Geochemistry**, v. 5–9, p. 225–272, 2003.

HENDERSON, P. General geochemical properties and abundances of the rare earth elements. **Rare Earth Element Geochemistry**, p. 1–32, 1983.

LACERDA, L. D. DE. Burial of mangroves by mobile dunes : a climate change threat in semiarid coasts. **ISME/GLOMIS Electronic Journal**, v. 16, n. 2, p. 6–10, 2018.

MERSCHEL, G. et al. Tracing and tracking wastewater-derived substances in freshwater lakes and reservoirs: Anthropogenic gadolinium and geogenic REEs in Lake Paranoá, Brasilia. **Comptes Rendus - Geoscience**, v. 347, n. 5–6, p. 284–293, 2015.

MINISTÉRIO DO MEIO AMBIENTE. **Caderno da Região Hidrográfica do Parnaíba**. Brasília: MMA, 2006.

PAULA FILHO, F. J. et al. Evaluation of water quality and trophic state in the Parnaíba River Delta, northeast Brazil. **Regional Studies in Marine Science**, v. 34, p. 101025, 2020.

SHABANI, M. B.; AKAGI, T.; MASUDA, A. Preconcentration of Trace Rare-Earth Elements in Seawater by Complexation with Bis(2-ethylhexyl) Hydrogen Phosphate and 2-Ethylhexyl Dihydrogen Phosphate Adsorbed on a C18 Cartridge and Determination by Inductively Coupled Plasma Mass Spectrometry. **Analytical Chemistry**, v. 64, n. 7, p. 737–743, 1992.

SHOLKOVITZ, E. R. The aquatic chemistry of rare earth elements in rivers and estuaries. **Aquatic Geochemistry**, v. 1, n. 1, p. 1–34, 1995.

ROUSSEAU, T. C. C. et al. Rare earth element analysis in natural waters by multiple isotope dilution-sector field ICP-MS. **Journal of Analytical Atomic Spectrometry**, v. 28, n. 4, p. 573–584, 2013.

5 CONCLUSÃO GERAL

Anomalias positivas de Gd foram observadas para a região costeira de Fortaleza. O gadolínio antropogênico tem origem na excreção renal de agentes de contraste a base de gadolínio utilizados em exames de ressonância magnética. A cidade já é fonte deste contaminante emergente para o oceano com seu emissário submarino descarregando aproximadamente 25 kg de Gd por ano.

Ao contrário do observado para Fortaleza, a região do Delta do Parnaíba não apresentou anomalias positivas de Gd, sugerindo que nela ainda não existem fontes antrópicas através da contaminação por esgotos.

Há uma remoção considerável dos ETRs dissolvidos nas salinidades de 0 a 6.4, comportamento semelhante ao já observado em outros estuários como o do Rio Amazonas.

REFERÊNCIAS ADICIONAIS

ALIBO, D. S.; NOZAKI, Y. Rare earth elements in seawater: Particle association, shale-normalization, and Ce oxidation. **Geochimica et Cosmochimica Acta**, v. 63, n. 3–4, p. 363–372, 1999.

BAU, M.; DULSKI, P. Anthropogenic origin of positive gadolinium anomalies in river waters. **Earth and Planetary Science Letters**, v. 143, n. 1–4, p. 245–255, 1996.

DEBERDT, S.; VIERS, J.; DUPRÉ, B. New insights about the rare earth elements (REE) mobility in river waters. **Bulletin de la Société Géologique de France**, v. 173, n. 2, p. 147–160, 2002.

DENG, Y. et al. Rare earth element geochemistry characteristics of seawater and porewater from deep sea in western Pacific. **Scientific Reports**, v. 7, n. 1, p. 1–13, 2017.

DUBININ, A. V. Geochemistry of rare earth elements in the ocean. **Lithology and Mineral Resources**, v. 39, n. 4, p. 289–307, 2004.

DE CAMPOS, F. F.; ENZWEILER, J. Anthropogenic gadolinium anomalies and rare earth elements in the water of Atibaia River and Anhumas Creek, Southeast Brazil. **Environmental Monitoring and Assessment**, v. 188, n. 5, 2016.

GAILLARDET, J.; VIERS, J.; DUPRÉ, B. Trace Elements in River Waters. **Treatise on Geochemistry**, v. 5–9, p. 225–272, 2003.

GARCÍA, M. G. et al. Sources of dissolved REE in mountainous streams draining granitic rocks, Sierras Pampeanas (Córdoba, Argentina). **Geochimica et Cosmochimica Acta**, v. 71, n. 22, p. 5355–5368, 2007.

GOLDSTEIN, S. J.; JACOBSEN, S. B. Rare earth elements in river waters. **Earth and Planetary Science Letters**, v. 89, n. 1, p. 35–47, 1988.

HENDERSON, P. General geochemical properties and abundances of the rare earth elements. **Rare Earth Element Geochemistry**, p. 1–32, 1983.

KULAKSIZ, S.; BAU, M. Anthropogenic dissolved and colloid/nanoparticle-bound samarium, lanthanum and gadolinium in the Rhine River and the impending destruction of the natural rare earth element distribution in rivers. **Earth and Planetary Science Letters**, v. 362, p. 43–50, 2013.

KÜMMERER, K.; HELMERS, E. Hospital effluents as a source of gadolinium in the aquatic environment. **Environmental Science and Technology**, v. 34, n. 4, p. 573–577, 2000.

LEYBOURNE, M. I.; JOHANNESSON, K. H. Rare earth elements (REE) and yttrium in stream waters, stream sediments, and Fe-Mn oxyhydroxides: Fractionation, speciation, and controls over REE + Y patterns in the surface environment. **Geochimica et Cosmochimica Acta**, v. 72, n. 24, p. 5962–5983, 2008.

MCLENNAN, S. M. Rare earth elements in sedimentary rocks: influence of provenance and sedimentary processes. **Geochemistry and Mineralogy of Rare Earth Elements, Reviews in Mineralogy 21**, p. 169–200, 1989.

MERSCHEL, G. **Trace Element and Isotope Geochemistry of Particle- Reactive Elements in River Waters of the Amazon River Basin**. [s.l.] Jacobs University, 2015.

MÖLLER, P. et al. Anthropogenic gadolinium as a conservative tracer in hydrology. **Journal of Geochemical Exploration**, v. 69–70, p. 409–414, 2000.

MORA, A. et al. Hydrological control, fractionation, and fluxes of dissolved rare earth elements in the lower Orinoco River, Venezuela. **Applied Geochemistry**, v. 112, 2020.

NOZAKI, Y. Rare Earth Elements and their Isotopes in the Ocean. **Encyclopedia of Ocean Sciences**, p. 2354–2366, 2001.

PIPER, D. Z.; BAU, M. Normalized Rare Earth Elements in Water, Sediments, and Wine: Identifying Sources and Environmental Redox Conditions. **American Journal of Analytical Chemistry**, v. 04, n. 10, p. 69–83, 2013.

ROUSSEAU, T. C. C. et al. Rapid neodymium release to marine waters from lithogenic sediments in the Amazon estuary. **Nature Communications**, v. 6, 2015.

SHOLKOVITZ, E. R. The aquatic chemistry of rare earth elements in rivers and estuaries. **Aquatic Geochemistry**, v. 1, n. 1, p. 1–34, 1995.

SHOLKOVITZ, E. R. Chemical evolution of rare earth elements: fractionation between colloidal and solution phases of filtered river water. **Earth and Planetary Science Letters**, v. 114, n. 1, p. 77–84, 1992.

SHOLKOVITZ, E. R. The geochemistry of rare earth elements in the Amazon River estuary. **Geochimica et Cosmochimica Acta**, v. 57, n. 10, p. 2181–2190, 1993.

SHOLKOVITZ, E. R.; LANDING, W. M.; LEWIS, B. L. Ocean particle chemistry: The fractionation of rare earth elements between suspended particles and seawater. **Geochimica et Cosmochimica Acta**, v. 58, n. 6, p. 1567–1579, 1994.

SHOLKOVITZ, E.; SHEN, G. T. The incorporation of rare earth elements in modern coral. **Geochimica et Cosmochimica Acta**, v. 59, n. 13, p. 2749–2756, 1995.

SMRZKA, D. et al. **The behavior of trace elements in seawater, sedimentary pore water, and their incorporation into carbonate minerals: a review**. [s.l.] Springer Berlin Heidelberg, 2019. v. 65

SONKE, J. E.; SALTERS, V. J. M. Lanthanide-humic substances complexation. I. Experimental evidence for a lanthanide contraction effect. **Geochimica et Cosmochimica Acta**, v. 70, n. 6, p. 1495–1506, 2006.

TACHIKAWA, K.; JEANDEL, C.; ROY-BARMAN, M. A new approach to the Nd residence time in the ocean: the role of atmospheric inputs. **Earth and Planetary Science Letters**, v. 170, n. 4, p. 433–446, 1999.

TANG, J.; JOHANNESSON, K. H. Speciation of rare earth elements in natural terrestrial waters: Assessing the role of dissolved organic matter from the modeling approach. **Geochimica et Cosmochimica Acta**, v. 67, n. 13, p. 2321–2339, 2003.